CEP162 Deficiency Causes Human Retinal Degeneration And Reveals A Dual Role In Ciliogenesis And Neurogenesis

by

Nafisa Nuzhat

A dissertation submitted in partial fulfillment
of the requirements for the degree of
Doctor of Philosophy
(Cell and Developmental Biology)
in the University of Michigan
2023

Doctoral Committee:

Professor Kristen Verhey, Chair
Professor Peter Hitchcock
Professor Ryoma Ohi
Assistant Professor Jillian Pearring
Assistant Professor Swathi Yadlapalli

Nafisa Nuzhat

nnuzhat@umich.edu

ORCID iD: 0000-0002-1744-4156

Dedication

This dissertation is dedicated to my family. I wouldn't be here writing this without your continuous support and duas. I am honored to be your granddaughter, daughter, sister, and wife. To my Basirah, my first pet, who started this journey with me but unfortunately passed away before we could cross the finish line together.

Acknowledgements

I'd like to start by thanking the entirety of Pearring lab. Thank you for your unyielding support and encouragement that made this possible. Thank you, Jason Willer, for being the best lab manager and for teaching me to speak up and ask for help. Thank you, Jorge, Molly, and Amanda; you all taught me how to be an irreplaceable resource and an ally in the lab. To Hanh Truong, my best friend, and my lab mate; thank you for being my dearest friend and for being my sounding board for life and science. To Dr. Pearring, thank you for giving me the space to grow and become the scientist that I am. The lab you created, and your mentorship gave me the confidence to carry out, write, and defend this dissertation. To my thesis committee members, thank you for lending me your time, advise, and expertise throughout this PhD Journey. This dissertation wouldn't have been possible without your foresight and scholarly support. To all my friends near and far, thank you for making time for me and for cheering me on no matter what phase of this PhD I was on. To my Ammu (mom), Abbu (dad), Baiya (brother), and Zoreen (sistern-in-law); thank you for being my safe space and for grounding me. Your sacrifice and unconditional love brought me here and I am forever grateful. To my Ammu and Abbu in particular, you left the warmth and familiarity of your motherland and immigrated to a foreign land that still struggles to accept you, for us. I hope you are proud. To my husband Oliver, you are my home. Your love, support, wisdom, and delicious home-cooked meals provided the balance I needed to prevent burnout and to continue towards my dreams.

Thank you for taking on so much while I wrote this dissertation and for your countless pep talks, this PhD is for you and your dreams as well. To my dearest fur babies, Basirah, Bella, and Bruno; thank you for bringing all the cuddles and joy into my life and for allowing me to love you. And finally, to God, my source of strength; without you there is no Nafisa. Everything is for you.

Table of Contents

List of Figures

Abstract

Primary cilia are antenna-like cellular organelles that protrude from the plasma membrane to detect extracellular signals and to regulate cellular physiology. They are present in virtually all post-mitotic cells and contribute to a wide array of signaling pathways required for development and tissue homeostasis. In the retina, photoreceptor neurons have adapted their primary cilia for detecting light and to propagate the visual response. Structural and functional defects in the cilia result in a spectrum of disorders, collectively termed ciliopathies. Over 200 clinical diagnoses have been associated with ciliary dysfunction and retinal degeneration appears in over half of these reported ciliopathies, emphasizing the importance of understanding how ciliary proteins are adapted for photoreceptor development and function.

As more ciliary genes are implicated in ciliopathies, one challenge in the field is determining how widespread (syndromic) or isolated (non-syndromic) ciliopathies manifest from a single gene mutation. While much is known about ciliogenesis and structural details about the primary cilia are actively studied, how these processes are evolutionarily adapted for photoreceptor function as well as mechanistic insights into how ciliary gene mutations contribute to syndromic and/or non-syndromic retinal degeneration remains unknown. Data presented in this thesis addresses these gaps in knowledge by investigating the role of CEP162 in the retina. CEP162 is a microtubule-associated centriolar protein required for cilia formation and is linked to terminal cell cycle withdrawal during retinal development.

My dissertation project was initiated through a collaboration with clinical geneticists who identified a homozygous recessive frameshift causing early truncation in the *CEP162* gene (c. 1935dupA (p. (E646R*5)) in two unrelated individuals with late-onset retinitis pigmentosa. I demonstrate that CEP162 is essential for photoreceptor cell survival during retinal development and that it plays a role in recruiting several transition zone proteins during ciliogenesis. Through *in vivo* and *in vitro* disease modeling, I found that the patient mutation in CEP162 results in the loss of its ciliary function while its developmental role remains intact, thus manifesting as a late-onset non-syndromic retinitis pigmentosa and not a syndromic ciliopathy.

Chapter 1 Exploring Primary Cilium Formation, Function, And Adaptation For Sensing Light

1.1 Introduction

Cilia are microtubule-based organelles that protrude from the cell surface to sense their extracellular environment and regulate cellular physiology. According to phylogenetics, these ancestral organelles are believed to have been present in the earliest known unicellular eukaryotic organisms[1,2], although their importance in cell signaling and sensory events were not realized until the late 1900s[3]. As signal sensors and transducers, cilia function in a vast number of signaling pathways, ranging from their role in Hedgehog signaling during embryo development[4,5] to transducing the light response in the retina[6,7]. There are two major types of cilia, motile and non-motile, both of which are membrane-bound microtubule-based organelles that extend from the centrosomes after the cells enter a quiescent state.

Cilia biology has fascinated scientists for centuries with the first morphological analysis dating back to 1835 for motile cilia and 1898 for primary cilia[3]. The use of transmission electron microscopy (TEM) paved the way for structural analysis of the cilium in various animal models including roundworms (*Caenorhabditis elegans*), mice (*mus musculus*), and unicellular green alga (*Chlamydomonas reinhardtii*)[8–10]. Recently, use of cryo-electron tomography (Cryo-ET) has provided greater resolution and further resolved the architecture of this tiny organelle[11–15]. There are three fundamental structural components to a cilium; a basal body, a transition zone (TZ), and an axoneme (Figure 1-

1). The basal body sits at the proximal end and contains a mother and daughter centriole, which are composed of 9 sets of triplet microtubules arranged in a cylinder. Each triplet consists of A, B, and C tubules as well as other proteinaceous structures that line the inside of the cylinder and a linker between the A-C tubules[16]. The mother centriole is distinguished from the daughter centriole by the presence of sub-distal and distal appendages (DA). These appendages form at the distal end of the mother centriole and are organized into a radial array of blade-like structures. The mother centriole serves as a nucleation site for the growth of the axoneme microtubules. The axoneme is made up of 9 sets of doublet microtubules and although the 9-fold symmetry is maintained, as the axoneme is extended, the doublet microtubules tapper into singlets of varying lengths near the distal tip of the cilium[11]. Adjacent to the basal body is a specialized region along the axoneme known as the transition zone which maintains ciliary composition and structural integrity (Figure 1-1).

While both motile and non-motile cilia share these structural similarities, in motile cilia the 9 sets of doublet microtubule are arranged around a pair of singlet microtubules at the center of the axoneme (9+2 conformation, Figure 1-1). Dynein arms and radial spokes project outward from each doublet microtubule towards this central pair apparatus and function in concert to drive cell motility. The inner dynein arms are thought to facilitate bending of the axoneme[17], while conformational change of the outer dynein arms in response to ATP hydrolysis generates the beat[17,18]. Motile cilia are found on many epithelial cells lining the respiratory tract[19], oviduct[20], and spinal cord[21] where they rapidly beat in a whip-like fashion to sense fluid flow and facilitate fluid clearance. During vertebrate development, the rotational movement of nodal cilia found in the nodal cavity

is critical for detecting the flow of signaling molecules and establishing left-right asymmetry[22]. Motile cilia are also observed in vertebrate sperm[23] and in *Chlamydomonas*[24,25] where they act as chemo-sensors and drive cell motility.

Primary cilia do not contain the central pair of microtubule filaments and are therefore arranged in a 9+0 conformation (Figure 1-1). Almost all post-mitotic vertebrate cells extend a primary cilium to detect extracellular signals, while sensory neurons in the eyes, nose, and ears have adapted their cilium to sense environmental ques, such as light, odorants, and sound wave[26–28]. Apart from their specialized role in sensory tissues, primary cilia were originally considered to be vestigial organelles until the early 20th century, when their functional loss was connected to polycystic kidney disease (PKD)[29].

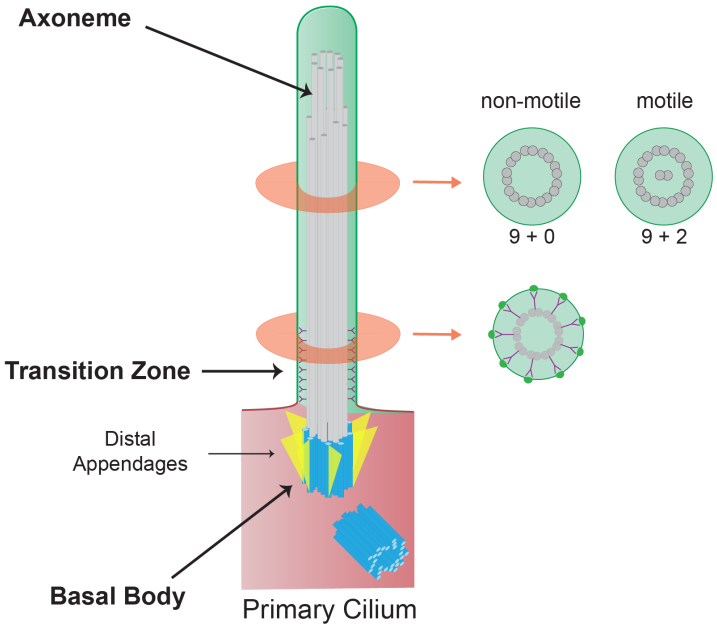

Figure 1-1 The architecture of the primary cilium.

At present, an online repository containing a compiled list of known ciliary components identified 686 genes involved in cilia formation. Of these genes, 539 genes encode core ciliary proteins essential for cilium formation, function, and survival. This

chapter will explore how primary cilia are assembled for function, and how defects in the cilium produce ciliopathies. It will also address how this unique organelle was adapted to function in retinal photoreceptors to detect photons of light that enter the eye and identify CEP162 as a ciliary protein with potential function in outer segment integrity and retinal development.

1.2 Ciliogenesis is a tightly regulated multistep process

Ciliogenesis is a highly conserved process by which a large network of proteins is recruited in a spatiotemporal manner to assemble a mature cilium. Hundreds of genes are implicated in this process and core components of cilia formation are well conserved amongst numerous eukaryotic species. In vertebrate cells, two separate pathways have been described for the process of cilia assembly: extracellular and intracellular. The extracellular pathway, observed in polarized epithelial cells, begins with modification of the mother centriole into a basal body which docks directly to the plasma membrane[30]. In contrast, the intracellular pathway begins in the cytoplasm and fusion to the plasma membrane doesn't occur until after a large ciliary vesicle is formed[31]. I will largely focus on primary cilia assembly through the intracellular pathway as human fibroblasts, retinal

pigment epithelial cells (RPE), and photoreceptors have all been shown to utilize this pathway (Figure 1-2).

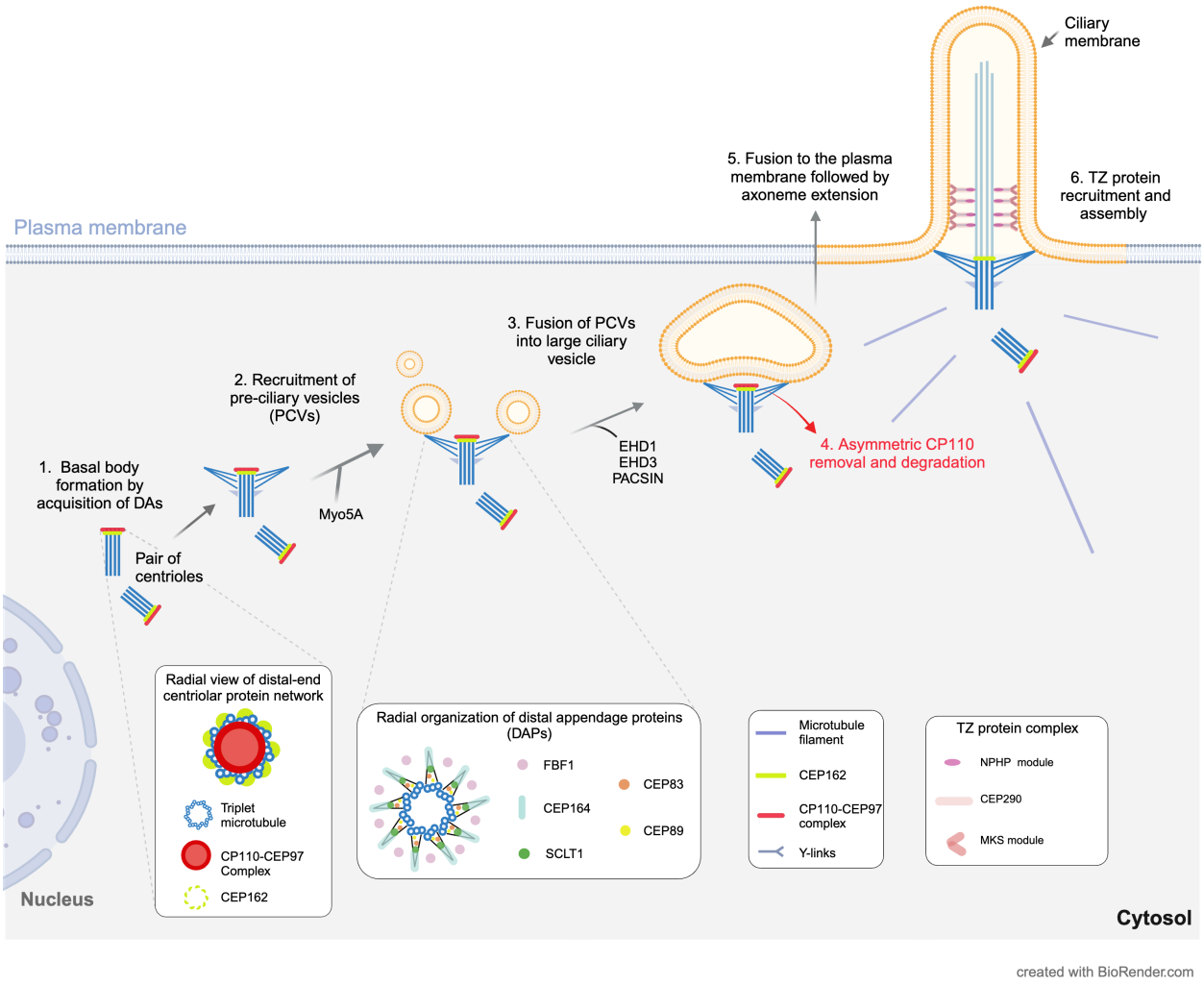

Figure 1-2 Ciliogenesis is a complex multistep process.

Pathway adapted from Wang et al, 2013; Reiter and Leroux, 2018; Kumar and Reiter, 2021 [149,197,198]

At the onset of cell cycle exit, the mother centriole recruits distal appendage proteins (DAPs) in a hierarchical order (CEP83, CEP89, SCLT1, FBF1, and CEP164) to form the DAs[32–37]. Once the DAs are attached to the mother centriole, the newly matured basal body recruits two small GTPases, Rab8 and Rab11, which are subsequently activated by the guanine exchange factor (GEF) Rabin 8 to promote and regulate the trafficking of pre-ciliary vesicles (PCVs) to the basal body[38–40]. Myosin5A, which is an

actin-based motor protein, transports the PCVs to the DAs[41] where CEP164 mediates their docking to the basal body[42]. These PCVs are then fused together by membrane remodeling proteins EHD1, EHD3, and RAB34 to form the large ciliary vesicle[43–45]. Recently, PACSIN proteins that contain an F-BAR domain and EHD1, have been implicated in forming extracellular membrane tunnels that extend from the ciliary vesicle to the plasma membrane[46]. Although these membrane tunnels have been identified, the molecular mechanism underlying their formation and how the ciliary membrane fuses with the plasma membrane remains unknown.

Extension of the axoneme, which is nucleated from the microtubule A and B tubule of the basal body, is the final stage of ciliogenesis[47,48]. As a cilium does not possess biosynthetic function of its own, axonemal subunits, membrane remodeling proteins, and resident ciliary proteins must be transported to the base of this growing structure. Intraflagellar transport (IFT) machinery, which were first discovered in the flagellar axonemes of *Chlamydomonas*[49], move bi-directionally carrying ciliary cargo such as axonemal subunits[48]. Functional studies impairing IFT movement in *Chlamydomonas* and *C-elegans* abolished ciliogenesis altogether[50–52], suggesting that movement of IFT machinery is essential for cilia assembly. As the axoneme is nucleated, TZ is delineated by recruitment of macromolecular protein complexes to that region. These proteins organize into two distinct modules: nephronophthisis (NPHP) and meckel (MKS) modules[53–55]. The NPHP module is composed of proteins NPHP1, NPHP4, and RPGRIP1L[56–58]. The MKS module is composed of transmembrane proteins (TMEM67, TMEM216, TMEM17, TMEM231, TMEM107), tectonic proteins (TCTN1, TCTN2, TCTN3), coiled-coiled proteins (CC2D2A, CEP290, AHI1), and B9 domain proteins

(MKS1, B9D1, B9D2)[54,58–64]. These modules further associate with one another forming a molecular meshwork known as the “Y-links”, which are thought to provide structural support by tethering the axoneme to the ciliary membrane[65,66]. While the precise function of the TZ “Y-links” remains debated, this basal region of the cilium is known to regulate the enrichment of ciliary resident proteins within the cilium[53,59,65,67]. For a comprehensive review of the discovery and function of TZ proteins and their role as a ciliary gate, please refer to these reviews[53,68].

1.2.1 Regulation of ciliogenesis involves removal of CP110 and accumulation of MARK4

Cilia assembly, at the stage of axoneme extension, is a heavily regulated step with recruitment and function of multiple protein complexes that converge to either prevent or promote building of the axoneme (Figure 1-3). KIF24 is part of the kinesin-13 family of motor proteins and localizes to the distal end of centrioles throughout cell cycle where it recruits the CP110-CEP97 complex[69]. CP110-CEP97 complex is essential for centriolar duplication[70,71] and to prevent premature cilia assembly[72–74]. KIF24 positively regulates ciliogenesis by promoting the removal of the CP110-CEP97 complex asymmetrically from the mother centriole[69]. Tau-Tubulin Kinase 2 (TTBK2) is a microtubule tracking kinase that is recruited to the centriolar distal end by CEP164[75] and also shown to be essential for CP110 removal[76]. After formation of the large ciliary vesicle, KIF24 recruits MPP9 which binds to CEP97 forming a CP110-CEP97-MPP9 complex. TTBK2 phosphorylates MPP9, allowing for the removal of the CP110-CEP97 complex from the mother centriole. Once removed, the complex undergoes ubiquitin-mediated proteasome degradation[77]. Microtubule affinity regulating kinase 4 (MARK4) is part of the serine/threonine kinase

family with established roles in regulating ciliogenesis[78], cell polarity[79], and asymmetric neural cell division[80]. Prior to axoneme extension, MARK4 partially recruits and phosphorylates centriolar subdistal appendage protein ODF2. When MARK 4 is depleted, ODF2 centriolar localization is lost, resulting in impaired axoneme extension and persistence of CP110 at the mother centriole[78]. How these regulatory components are recruited in a time sensitive manner and whether accumulation of MARK 4 directly contributes to CP110 removal remains to be determined.

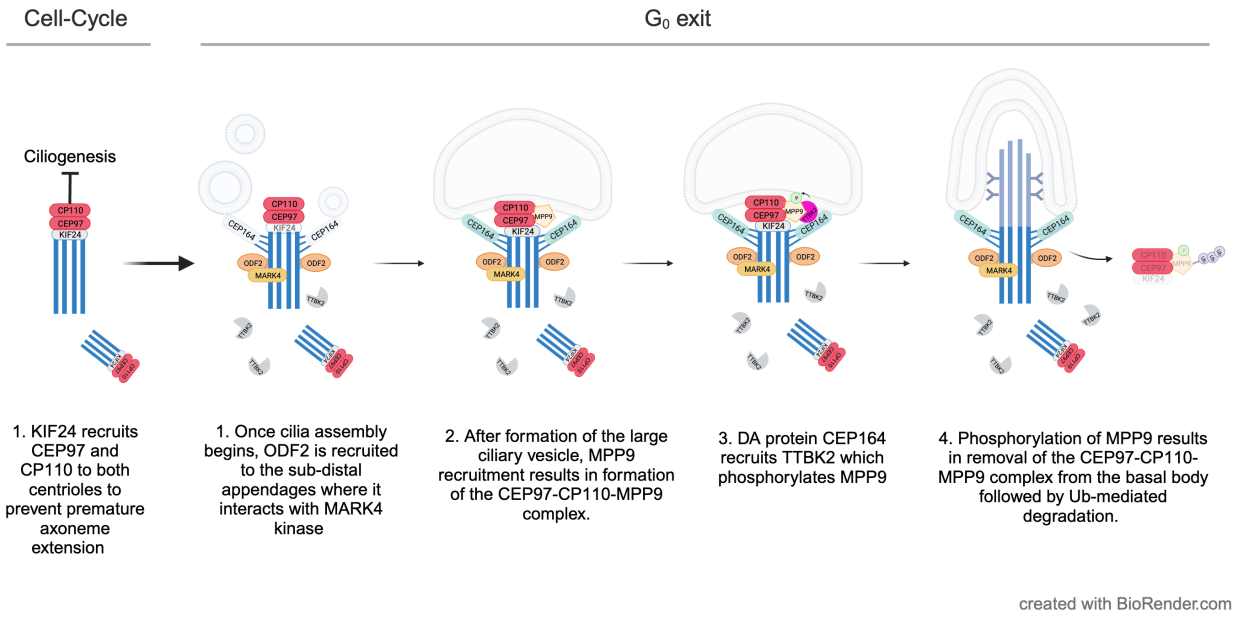

Figure 1-3 Ciliogenesis is regulated by CP110 removal and accumulation of MARK4

Pathway adapted from Kobayashi et al, 2011; Huang et al, 2018; Kuhn et al, 2013; Cajanek et al, 2014[69,75,77,78]

1.3 Adaptation of primary cilia as sensors of light

Once fully extended, diverse signaling roles of the primary cilia are influenced by its membrane protein composition. The ciliary membrane is enriched with signaling receptors such as Hedgehog and Wnt receptors which are crucial for sensory functions during embryo development[4,81,82]. In the retina, sensory cells like the photoreceptors

contain specialized cilia that incorporate signaling receptors such as opsins into their membrane to detect and transduce the visual response[7,83].

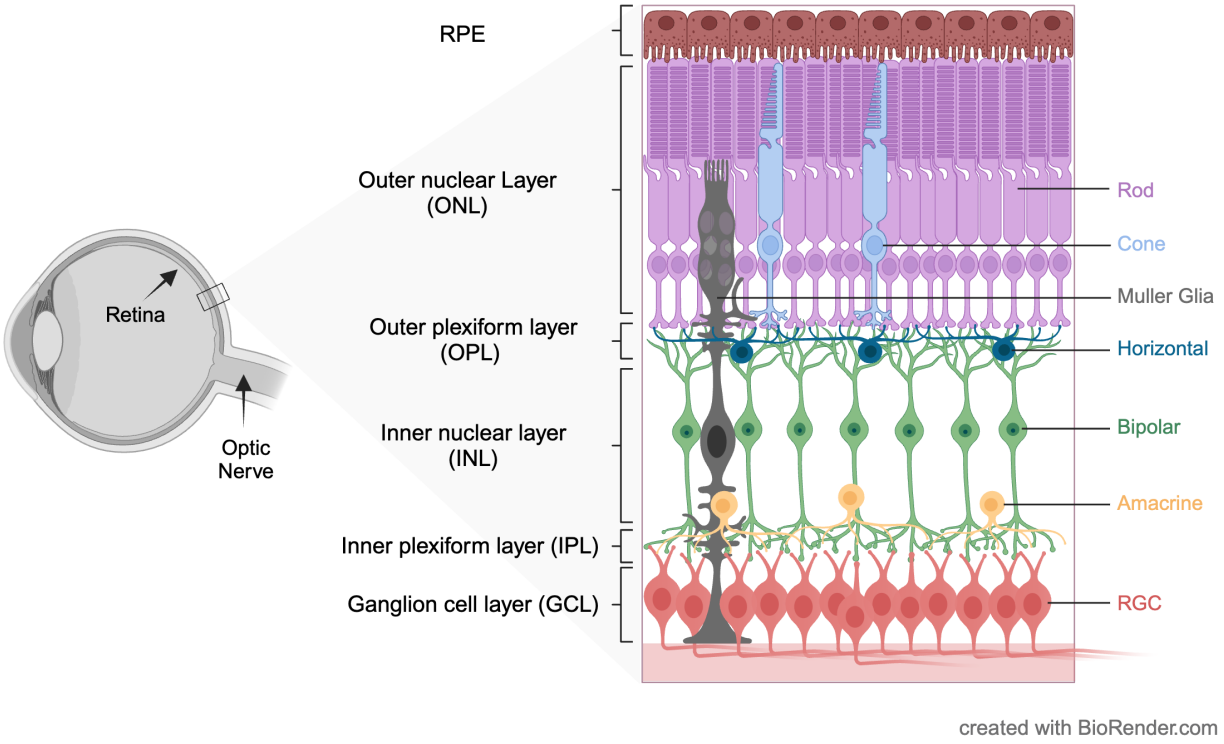

Figure 1-4 Organization of the retina.

Adapted from Cepko, 2015[93]

1.3.1 Vertebrate retina is a highly organized and layered tissue

The vertebrate retina is a thin layered tissue organized precisely to detect and process complex visual cues. It is comprised of five classes of neurons and one class of glial cell, all of which are organized into three nuclear layers and two plexiform layers where synapses are formed[84,85] (Figure 1-4). In the outer retina, the light-sensing outer segments of photoreceptor cells are adjacent to the RPE. The photoreceptor nuclei make up the outer nuclear layer (ONL), while their axon terminals extend into the outer plexiform layer (OPL). The inner nuclear layer (INL) houses cell bodies of bipolar, horizontal, and amacrine cells, which form synapses in the inner plexiform layer (IPL) with retinal ganglion

cells (RGCs) in the ganglion cell layer (GCL). Ganglion cell axons form the optic nerve which conveys the visual output to the brain. Müller glia are specialized radial glia that span almost the entire length of the retina and support the metabolic, homeostatic, and functional activities of the neurons[86].

Early lineage tracing experiments in various animal models revealed that retinal progenitor cells (RPCs) give rise to all the cells in the retina. RPCs are multipotent, in that during development, a single RPC cycles through stages of competency in a highly conserved and sequential process to produce these diverse cell types. This competency model is further supported by decades of research showing cell intrinsic and extrinsic factors that influence how RPCs generate and maintain proper ratios of individual cell types in the retina[87–90]. The developmental window varies between species, but the birth order of the neurons is conserved and proceeds in a central-to-peripheral gradient[91]. In mice, RGCs are born first at E12.5, along with cones and horizontal cells[90,92] (Figure 1-5). While amacrine cells share the same birthdate with cones and ganglion cells, it extends beyond and continues until P2. Rods are born between E12.5 and P7 with peak development at P0. The last set of cells to be born are bipolar cells and Müller glia which

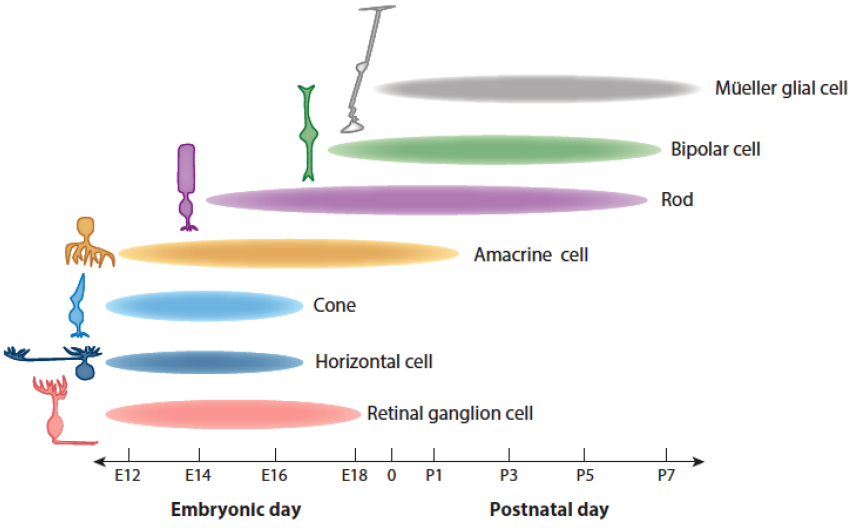

Figure 1-5 Retinal neurons are born in a highly conserved and sequential manner.

Adapted for publication with permission from Cepko, 2015[93]

are born concurrently between P0 and P7[93]. A comprehensive overview of how cells establish individual identity and how RPCs are regulated during this process of cell fate determination can be found in the following reviews.[91,93,94]

1.3.2 Photoreceptor cells are polarized neurons containing a light-sensitive ciliary compartment

Photoreceptors are critical for light detection and subsequent processing of the light response. There are two kinds of photoreceptor cells: rods and cones. Cones are used for high acuity and color vision and rods are responsible for high-sensitivity detection at low-light conditions. As the most abundant cell type in the mammalian retina, rods vastly outnumber every other cell type. In humans, there are approximately 120 million rods and only 6 million cones[95]. In the mouse retina, 72% of neurons are rods while cones only make up 2.2%[90].

As polarized neurons, photoreceptors are organized into four major sub-compartments: the outer segment, the inner segment, the nucleus, and the synapse (Figure 1-6). Located most distally, the outer segment is a membrane-dense organelle that houses all the components for light detection and signal propagation. When a photon of light is absorbed, 11-cis-retinal bound to opsins in both rod and cones is isomerized to all-trans-retinal. This induces a conformational change within the opsins that activates a G-protein and begins an intracellular signaling pathway that culminates in the closure of cyclic nucleotide-gated channels located within the outer segment plasma membrane and hyperpolarization of the photoreceptor[96]. To maximize light absorption and signal propagation, opsins and signaling proteins are densely packed within ~800-1000 membrane discs which are stacked tall to form the large outer segment compartment[97].

While in cone outer segments, the discs remain contiguous with the plasma membrane, in rods these discs are self-contained flattened vesicles[98,99].

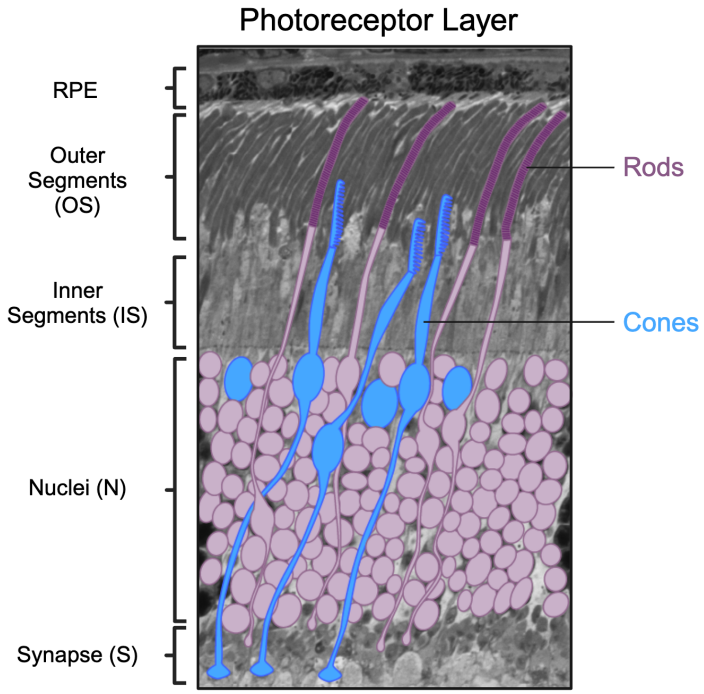

Figure 1-6 Photoreceptors are polarized neurons with distinct sub-compartments.

Even though the outer segment is specialized for light detection and shares core features with the primary cilium, such as the basal body, TZ, and the axoneme, a notable distinction arises at their TZ regions. Photoreceptor TZs, commonly referred to as connecting cilia, are five times larger than their primary cilia counterpart. In Addition to localization of known TZ proteins such as NPHP1, NPHP4, TMEM67, and CEP290 to the connecting cilium[100], photoreceptor-specific ciliary proteins such as RPGRIP1[101], RPGR-ORF15[102], and Spata7[103] also get recruited to this region.

The connecting cilium bridges the light-sensitive outer segment to the rest of the cell body and ensures proper compartmentalization of signaling proteins within the ciliary outer segment. The inner segment sits apical to the nucleus and contains all housekeeping organelles required for the metabolic and biosynthetic activity of the cell. At the most proximal end, photoreceptors form synapses with the inner retinal neurons to propagate the visual response.

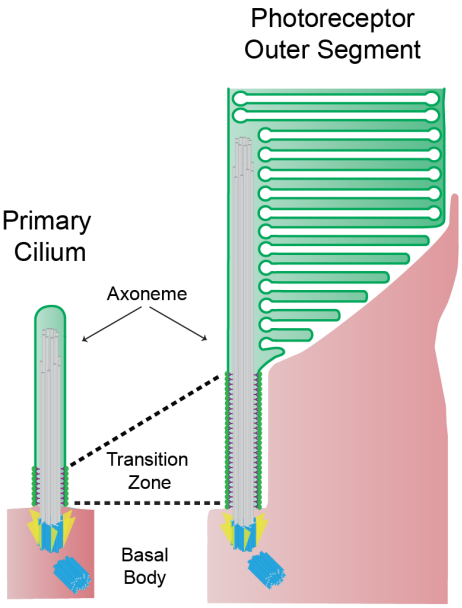

Figure 1-7 Photoreceptor outer segment is a specialized cilium that shares core structural elements with the primary cilium.

1.3.3 Photoreceptor outer segment development and renewal

In mouse photoreceptors, outer segment formation starts around P7, and the initial steps of this process closely resemble the early stages of intracellular primary ciliogenesis[90,104–106]. After cell-cycle exit, the mother centriole matures into a basal body as it acquires distal and sub-distal appendages[104]. More recently, localization of CEP164 at the distal appendages was observed using expansion microscopy[107], and shown to be required for outer segment development and recruitment of IFT complexes in mouse rod

photoreceptors[108]. According to TEM analysis in the developing mouse retina, pre-ciliary vesicles are recruited to this newly matured basal body where they are fused together to form a large ciliary vesicle. This large ciliary vesicle then docks to the apical plasma membrane where membrane remodeling proteins drive its fusion[104]. As the ciliary membrane grows, axoneme is also extended to form the connecting cilium. Presence of periodic bead-like intramembrane particles, termed the ciliary necklace, observed through freeze-fracture electron microscopy is a structural hallmark of the connecting cilium[109].

The subsequent stages of outer segment formation diverge considerably from that of primary cilia due to the building of disc membranes[110]. Disc formation occurs distal to the connecting cilium and is initiated by branched actin polymerization pushing out the ciliary membrane[110,111]. The subsequent steps include disc elongation, disc flattening, and, in rods, disc enclosure. The outer segment is filled with ~800-1000 flattened disc membranes, and every day new disc membranes are added to the outer segment base, while old discs are phagocytosed from the outer segment tip. Continuous renewal of the outer segment is critical for maintaining healthy photoreceptors and defects in disc morphogenesis are known to cause photoreceptor cell death and blindness in humans[112]. While structural and scaffolding proteins have been localized to disc membranes and implicated in outer segment integrity[113], the precise molecular mechanism underlying disc formation remains an active area of study.

1.4 Discovery and characterization of Ciliopathies

Ciliopathies are human diseases characterized by structural and/or functional defects in motile and/or primary cilia. These inherited diseases are rare and can present with a wide variety of symptoms from polydactyly to kidney disease depending on the organ

system(s) involved. Global databases like SYSCILIA[114], CILIACARTA[115], and Cilia Miner[116] were established to consolidate this ever-growing list of genes, which now include over 200 causal genes. The molecular mechanism underlying the disease pathogenesis, clinical symptoms, and severity depend on how the genetic mutations manifest in specific tissues. A single ciliary gene mutation could present with either syndromic disease affecting multiple tissues, or non-syndromic disease in an isolated tissue.

Motile ciliopathy is ciliary dysfunction attributed to the loss of ciliary locomotion and many of these mutations affect the formation and function of inner and outer dynein arms that are critical for ciliary motility[117,118]. While some of these ciliopathies manifest in isolated tissue, like left-right patterning defects (situs inversus) caused by dysmotility of the nodal cilia during development, others like primary ciliary dyskinesia can affect multiple organs such as the lungs, nose, and ears[119,120]. For an in-depth analysis of motile ciliopathies, please refer to this review by Wallmeier and colleagues[121].

The sensory capability of the primary cilium depends on the enrichment of membrane-bound signaling proteins within the ciliary membrane during ciliogenesis. As such, defects in the formation and function of the primary cilia result in various forms of ciliopathies. Single mutations in distal appendage proteins such as CEP164 and CEP83, which are required for ciliogenesis, result in syndromic disorders such as Nephronophthisis (NPHP) and are often accompanied by intellectual disabilities[122,123]. Similarly, the persistence of CP110 at the mother centriole during ciliogenesis due to impaired localization and function of TTBK2[76], MARK4[78], and CEP78[124] is implicated in syndromic ciliopathies such as Meckel syndrome (MKS) and Joubert syndrome (JBTS).

The TZ of the cilium, the region responsible for maintaining ciliary membrane protein composition and structural integrity, is considered a hotspot for ciliopathies with mutations in at least 18 TZ proteins currently identified[53]. While mutations in some TZ proteins such as TMEM67 and CEP290 result in multi-organ disorders like MKS and JBTS[125–127]; other mutations in TZ proteins such as RPGR-ORF15 and RPGRIP1l are implicated in non-syndromic retinal ciliopathy[102,128–130].

1.4.1 Retinitis Pigmentosa is an inherited form of retinal ciliopathy

Retinal degeneration (RD) is a large genetically diverse group of disorders that cause vision impairment in children and adults. It is organized into three main categories: retinitis pigmentosa (RP), leber congenital amaurosis (LCA), and age-related macular degeneration (AMD). RP is one of the inherited forms of RD characterized by multiple factors including genetic mutations in genes encoding proteins essential for photoreceptor structure, function, biosynthesis, and survival[131–134]. RP clinically manifests as night blindness due to rod photoreceptor cell death, followed by loss of central vision when cone photoreceptors are affected, ultimately resulting in complete blindness. Range of severity, age-onset of the disease, and progression through the stages of RP are all variable amongst patients and depend on the genetic mutation itself. According to an online repository, known as retina information network, which catalogs all known genetic mutations causing RD (RetNet, https://sph.uth.edu/retnet/), at least 281 genes are currently identified and of those, 69 of them are linked to RP. Majority of these mutations are clinical reports with molecular basis for disease onset largely unexplored[135]. Genetic mutations extensively studied include genes encoding proteins that localize to the connecting cilium, which account for ~ 25% of RP cases and often manifest as syndromic

RP. CEP290 is a protein that localizes to the TZ of primary cilium and the photoreceptor connecting cilium with involvement in multiple components of cilium assembly. Mutations in it are associated with LCA, JBTS, NPHP, and MKS[127]. However, mutations in some TZ genes have also been linked to non-syndromic RP. Recently, CEP78, which encodes a centriolar protein known to function during cell division[136] and ciliogenesis by controlling CP110 levels[124], was identified as causing non-syndromic RP with no mechanistic insight into disease progression reported[137].

Retinal degeneration appears in over half of the genes associated with ciliopathies, and mutations in some of these ciliary proteins cause photoreceptor cell death exclusively[131,138]. In order to understand the diversity in retinal ciliopathy phenotypes, we must investigate their role in photoreceptor outer segment development and function. Moreover, ciliary genes are also implicated in additional cellular events such as centriole duplication, cell cycle, and neural migration[114,139–141]. So, it is imperative to take a "whole cell" approach when studying ciliary gene defects as ciliary proteins could contribute to other cellular mechanisms.

1.5 CEP162 is a microtubule-associated centriolar protein implicated in ciliogenesis and neurogenesis

Centrosomal proteins, or CEPs, are primarily localized to the centrioles and participate in various cellular processes including cell division, ciliary signaling, and ciliogenesis[70,136,142–144]. Thus, it is not surprising that mutations in many CEPs are linked to both ciliary and cell-cycle defects.

Quail neuroretina 1 (QN1) is an ortholog of CEP162 and was originally identified in quail neuroretinal cell clones (K2 cells) undergoing terminal cell division to generate

mature neurons[145]. *In situ* hybridization in quail retinal sections and isolated retinal cell cultures revealed high levels of QN1 mRNA transcripts in post-mitotic neurons. QN1 knockdown in the K2 cell clones led to an increase in cells going through S phase, as quantified by BrdU incorporation, suggesting it is important for the growth arrest of neurons[145]. Similarly, in chick retinal explants, knockdown of QN1 during terminal divisions also resulted in an increase in BrdU labeled cells. *In vivo* knockdown of QN1 during chick retinal development caused retinal dysplasia further validating its importance in promoting terminal cell division[146]. QN1 was found to share sequence homology with its human ortholog KIAA1009[147] and antiserum created against QN1 recognized both QN1 and KIAA1009 protein levels in cultured neural cells (PC12) that terminally divide upon addition of nerve growth factor (NGF)[148]. QN1/KIAA1009 associates with α-tubulin and localizes to the mitotic organizing center (MTOC) throughout mitosis in PC12 cells. It was postulated to play a role in chromosome segregation as QN1/KIAAA1009 knockdown caused defects in spindle assembly, microtubule polymerization, and elevated apoptosis in these cells. Although no direct analysis of its role in chromosome segregation was shown, whether this potential role is specific to terminally dividing neurons was tested by knocking down QN1/KIAA1009 in human epithelial breast cancer (MCF7) cells which resulted in increased apoptosis[148]. As no cell-cycle defects were reported in MCF7 cells, it remains unclear whether this potential role in chromosome segregation is neuron specific.

KIAA1009 was later identified using a mass spectrometry approach that differentially labeled modified and unmodified centrioles during S-phase to identify core centriolar proteins. Among the nine proteins identified, KIAA1009 alone was shown to

bind microtubules and was further classified as a distal end centriolar protein based on its subcellular localization, thereby renamed CEP162[149]. Functional studies in zebrafish *in vivo* showed that morpholino knockdown of *cep162* during zebrafish development caused a series of abnormalities associated with ciliary dysfunction. In cell culture, endogenous CEP162 localized to the distal ends of centrosomes throughout the cell cycle and at the basal bodies in ciliated cells, respectively. A series of truncation mutations in CEP162 revealed that it utilizes coiled-coiled (CC) domains on its C-terminus to interact with microtubules and centrioles independently of one another. Microtubule binding was restricted to CC1 and CC2 domains as overexpression of full-length CEP162 and a truncation construct containing both CC1 and CC2 domains directly bound taxol stabilized microtubules during microtubule pelleting assay. CC2 and CC3 are required for centriole localization as deletion of CC3 or overexpression of CC3 alone both abrogated centriolar localization. In cycling RPE1 cells, CEP162 consistently localized to the MTOC and the mitotic spindles, although transient knockdown of *CEP162* using siRNA did not affect the cell cycle, as previously seen by Leon and colleagues[148]. During ciliogenesis, the knockdown of CEP162 caused a significant reduction in percent ciliation, revealing an important ciliary function. In the absence of CEP162, early steps of ciliogenesis occurred normally including the removal of CP110; however, TZ proteins such as TMEM67, NPHP1, CC2D2A, and TCTN2 were not recruited to the base of the cilia. Overexpression of constructs containing the CC1 and CC2 domains of CEP162 caused the protein to localize along the entire axoneme and resulted in abnormal recruitment of TZ proteins to the tip of the cilia. This suggested that the CC2 and CC3 domains of CEP162 are used to tether it to the centrioles where it recruits TZ proteins to the cilium during ciliogenesis.

Moreover, CEP162 was shown to directly interact with CEP290 using its CC1 and CC2 domains. Localization of CEP290 to the mitotic spindles during mitosis and the TZ during ciliogenesis were shown to be dependent on its interaction with CEP162[149].

While CEP162 and its ortholog QN1 were studied with respect to ciliogenesis and terminal neural divisions, human mutations had not been reported in any clinical databases pertaining to neurodegenerative disease and/or ciliopathies.

1.6 Rationale and Approach

Primary cilia function like molecular antennae where they receive and process extracellular signals and regulate cellular physiology. Retinal photoreceptors have one of the largest sensory cilia in our body responsible for detecting light and propagating the visual response. While unique tissue-specific proteins are expressed in the photoreceptor cilium, expression and localization of core ciliary protein is also conserved. Consequently, ciliopathies often encompass retinal degeneration that ultimately results in blindness in patients.

CEP162 is a microtubule-associated centriolar protein required for ciliogenesis and is believed to also function in terminal cell-cycle exit during neurogenesis[145,146,148,149]. My dissertation was initiated through a collaboration with two clinical geneticists who identified a homozygous recessive frameshift causing early truncation in the *CEP162* gene (c. 1935dupA (p. (E646R*5)) in two unrelated patients with late-onset non-syndromic RP. Research presented in this dissertation will classify CEP162 as a novel retinal ciliopathy gene and investigate how this mutation induces non-syndromic manifestation of the disease in the patients. It will also investigate the role of CEP162 in

retinal development, which highlights an emerging perspective on the non-ciliary function of centriolar proteins.

Aim 1: Determine how the human E646R*5 mutation affects the expression, localization, and function of CEP162 in cell culture.

The patient mutation in CEP162, now referred to as CEP162-E646R*5, causes an early truncation removing nearly all 3 CC domains that were previously implicated in microtubule and centriole binding. In this aim, I primarily used patient-derived primary fibroblasts in combination with a variety of cellular and molecular biology techniques to test the expression, localization, and function of CEP162-E646R*5 compared to the full-length CEP162.

The CEP162-E646R*5 truncation retains only the first 29 amino acids of the CC1 domain, so I also determined whether the mutant protein could bind directly to microtubules by performing a microtubule binding assay with FLAG-CEP162-E646R*5 and full-length FLAG-CEP162. CEP162 was also shown to interact with CEP290 and promote its recruitment to the TZ in primary cilia. I created and purified FLAG-tagged CEP162 and FLAG-tagged CEP162-E646R*5 constructs that were then used for co-immunoprecipitation (co-IP) experiments to test direct binding of the truncated CEP162-E646R*5 to CEP290. Finally, advanced microscopy techniques such as correlative light and electron microscopy (CLEM) and TEM were employed to ascertain morphological defects in the primary cilia of patient fibroblasts compared to control fibroblasts. Super-resolution airy scan microscopy and immunofluorescence imaging provided cellular and molecular insights into how ciliogenesis was affected by this truncated mutation.

Aim 2: Investigate the function of CEP162 in the mouse retina.

CEP162 is a centrosomal protein that is also localized to the basal body as well as decorates the mitotic spindle during mitosis. It has previously been shown to play a role in initiating cellular quiescence in the developing chick retina. In this aim, I sought to understand how the CEP162 human mutation causes non-syndromic retinal dystrophy by investigating its function in the specialized light-sensitive photoreceptor cilium and during retinal development.

Using Cetn2-GFP transgenic mice, I determined the endogenous localization of CEP162 relative to other centriolar and ciliary proteins such as CP110 in the photoreceptor cells of the mouse retina. I used an *in vivo* subretinal electroporation technique to examine the localization of CEP162 in rod photoreceptors and its function in the retina by expressing shRNA knockdown and rescue constructs into the developing mouse retina at P0. Pycnotic nuclei quantification were performed in developing retinas to detect photoreceptor cell loss in response to the knockdown of CEP162 during retinal development.

Chapter 2 CEP162 Deficiency Causes Human Retinal Degeneration And Reveals Dual Roles In Ciliogenesis And Neurogenesis

Chapter 2 is a modified version of a manuscript published in the *Journal of Clinical Investigations*[150]. The following figures were modified from the manuscript and added as additional figures in the dissertation: Supplemental Figure 3: Figure 2-3, Supplemental Figure 4: Figure 2-6, Supplemental Figure 5: Figure 2-8, Supplemental Figure 6: Figure 2-7 and, Supplemental Figure 8: Figure 2-9. Additionally, Supplemental Figures 1, 2, 7, and 9 were not included as part of the dissertation.

2.1 Abstract

Defects in primary or motile cilia result in a variety of human pathologies, and retinal degeneration is frequently associated with these so-called ciliopathies. We show that homozygosity for a truncating variant in CEP162, a centrosome and microtubule-associated protein required for TZ assembly during ciliogenesis and neuronal differentiation in the retina, causes late-onset RP in 2 unrelated families. The mutant CEP162-E646R*5 protein is expressed and properly localized to the mitotic spindle but missing from the basal body in primary and photoreceptor cilia. This impairs recruitment of TZ components to the basal body and corresponds to complete loss of CEP162 function at the ciliary compartment, reflected by delayed formation of dysmorphic cilia. In contrast, rescue of increased cell death in the developing mouse retina after shRNA knockdown of *Cep162* by expression of CEP162-E646R*5 indicates that the mutant

retains its role for retinal neurogenesis. Human retinal degeneration thus results from specific loss of ciliary CEP162 function.

2.2 Introduction

Primary cilia are sensory organelles that protrude from the cell surface to detect extracellular signals that regulate cellular physiology. Cilia are highly dynamic microtubule-based organelles that are nucleated from the mother centriole and assembled and disassembled in each round of the cell cycle. The complex process of cilium assembly, maintenance, and disassembly is estimated to require thousands of genes, with nearly 700 transcripts confirmed to be localized to the cilium[114] and many more implicated in ciliary function. Dysfunction of ciliary genes and proteins is associated with a wide range of human disorders. These ciliopathies can involve virtually any organ, with particularly frequent affection of the retina. Proteins with established roles in cilia may also participate in other cellular processes. For example, OFD1, a centrosomal protein of the basal body implicated in non-syndromic RP and other syndromes[151,152], is also involved in chromatin remodeling[153] and cell cycle progression[154].

CEP162 was originally cloned from *QN1*[145]*.* Inhibition of QN1 during retinal development led to defective mitosis and differentiation suggesting that it is involved in withdrawal from cell cycle, so QN1 was postulated to play a role in neuronal quiescence[146,148]. QN1 is orthologous to human KIAA1009/CEP162[147], a protein that binds to microtubule spindles during mitosis and localizes to the distal ends of centrioles in post-mitotic cells[148,149]. Loss of CEP162 has been shown to arrest ciliogenesis at the stage of TZ assembly and to cause a ciliopathy phenotype in zebrafish[149]. Despite its

importance for cilia formation, no pathogenic *CEP162* variants have been reported in human disease, and its role in the retina has remained unknown.

Here, we show that homozygosity for a frameshift variant in *CEP162* causes late-onset RP in 2 unrelated families. We find that the truncated CEP162 is unable to localize to the basal body. Absence of CEP162 from the primary cilium results in a loss of some TZ components and delayed formation of dysmorphic cilia. However, truncated CEP162 maintains its capability to bind microtubules and localizes to the mitotic spindle, suggesting that it could retain function in neuronal cell division. Indeed, we find that increased cell death in the developing mouse retina with loss of *Cep162* expression can be restored not only by full-length, but also truncated CEP162 which is unable to localize to basal body in these cells. Thus, specific loss of CEP162 function at the primary cilium is likely the primary cause of the late-onset human retinal ciliopathy.

2.3 Results

2.3.1 Late-onset RP identified in 2 unrelated patients

Patient 1. Loss of visual acuity was noted at 56 years of age. At 60 years, RP was diagnosed. Night blindness had presumably pre-existed for years. There is now noticeable photophobia. At the age of 67 years, refraction revealed hyperopia and astigmatism in both eyes with +6.25 Sphere (sph), -1.25 Cylinder (cyl)/71° in the right eye and +2.75 sph, -1.00 cyl/58° in the left eye. Color fundus photography, blue light autofluorescence and spectral domain optical coherence tomography (OCT) were compatible with RP (pale optic disc, narrow vessels, bone spicule pigmentation, thinning of the outer nuclear layer; Figure 2-1A-F). Best corrected visual acuity (BCVA) was 20/500 for both eyes (Snellen chart), and visual fields were constricted. There was

synchysis scintillans in the right vitreous. *Patient 2.* Loss of visual acuity was reported since the 5th decade. At the age of 69 years, RP was diagnosed. BCVA was light perception (OD) and 4/10 (OS) and visual fields were constricted <10°. Color fundus photography showed a pale optic disk, narrow vessels with sheathing and limited bone spicule pigmentation. Fluorescein angiography displayed strong atrophy of the outer retina and few intraretinal pigment migrations. OCT showed absence of the outer retina, except in the fovea. On blue light autofluorescence, a Bull's eye aspect was observed. A pattern electroretinogram (ERG) showed an absent response (OD) and reduced macular function (OS) (Figure 2-1G-N). A full-field ERG could not be conducted. Patient 2 was followed at the diabetes clinic for 30 years; no islet cell autoantibodies were detected. There was a low normal production of C-peptide (0.20 nmol/L. Ref: 0.29-0,99 nmol/L). He received medication for chronic renal insufficiency due to diabetic nephropathy.

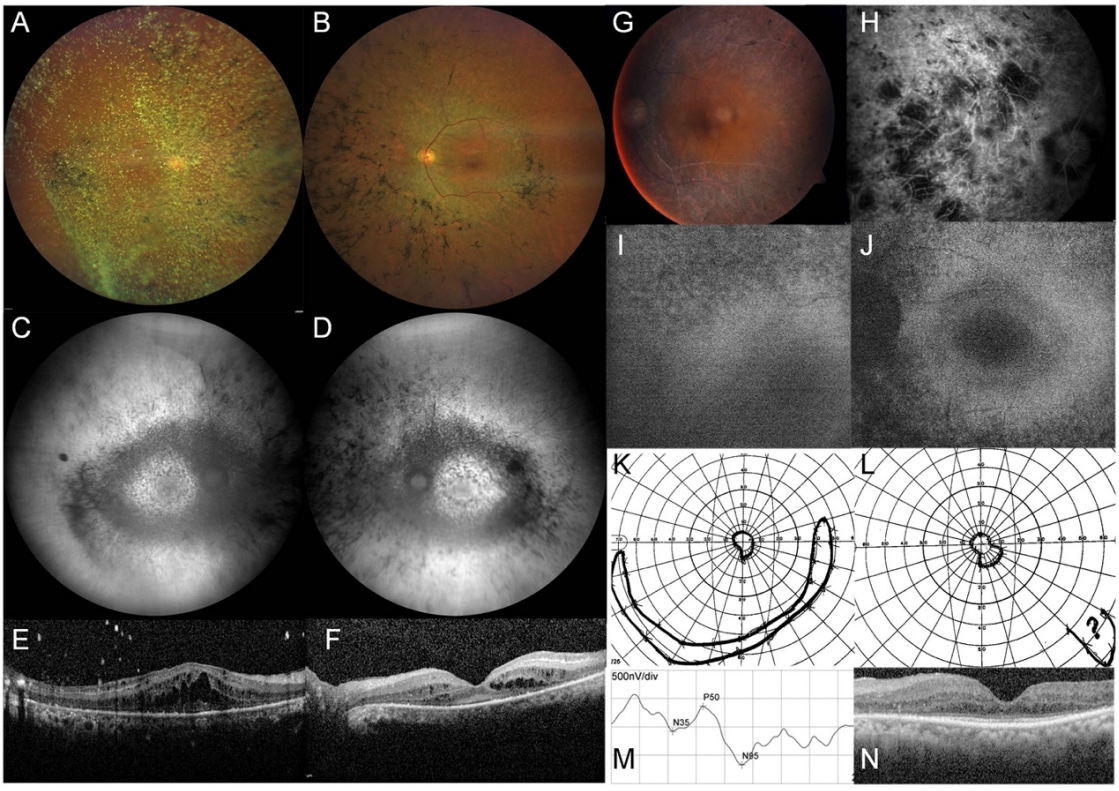

Figure 2-1 Ophthalmological data of patients 1 and 2 with RP.

A. *Right eye (OD) and* ***B.*** *left eye (OS) with pale optic disc, narrow vessels, and bone spicule pigmentation on color fundus photography.* ***C and D.*** *Granular decreased autofluorescence throughout the posterior pole on blue light autofluorescence.* ***E and F.*** *Spectral domain optical coherencetomography (SDOCT): Cystoid spaces in the inner and outer nuclear layer and thinning of the outer nuclear layer with sparing of the central fovea.* ***G.*** *Color fundus photography of the left eye: Pale optic disc, narrow vessels with pronounced sheathing giving a white, pseudothrombotic, aspect, bone spicule pigmentation.* ***H.*** *Fluorescein angiography of the right eye: Strong atrophy of the outer retina and few intraretinal pigment migrations. Autofluorescence from* ***I.*** *right eye and* ***J.*** *left eye: bull's eye aspect of the macula. Goldmann visual fields for* ***K.*** *left eye and* ***L.*** *right eye: constriction of < 10°.* ***M.*** *Pattern ERG of left eye: Reduced macular activity (visual acuity 3/10). No responses for the right eye.* ***N.*** *Optical coherence tomography: Absence of the outer nuclear layer beyond the macula.*

Abdominal ultrasound and CT showed no kidney abnormalities, but a lipomatous aspect of the pancreas. Patient 2 suffered from coronary main stem stenosis (50-59%, non-invasive treatment) and died at the age of 74.

2.3.2 Homozygous CEP162 frameshift variant in both unrelated RP patients

Patient 1 and Patient 2 were both born to consanguineous parents in 2 unrelated Moroccan families (Figure 2-2A). The grandparents of Patient 1, a 68-years old male, are 2nd degree cousins. No pathogenic variant was identified in Patient 1 by targeted NGS of 204 known IRD genes. WES generated 16.3 Gb of sequence, covering 97.9% of target sequence >30x. Among 701 rare variants, 41 were homozygous, further narrowed to 25 by applying an MAF of <1%, excluding artifacts and filtering with ROH. 24 variants were disqualified as RP-causing due to 1 or several of these reasons: a) Gene associated with an unrelated disease, b) homo- or hemizygous individuals in gnomAD, c) variant predicted as neutral/benign. 1 variant remained, a 1-base pair insertion in exon 15 of *CEP162*, NM_014895.3: c.1935dupA, causing a frameshift and premature nonsense codon (p.(Glu646Argfs*5), subsequently designated as E646R*5; Figure 2-2B, D). In the

other annotated *CEP162* isoform, the insertion corresponds to NM_001286206.1: c.1707dup, p. (Glu570Argfs*5).

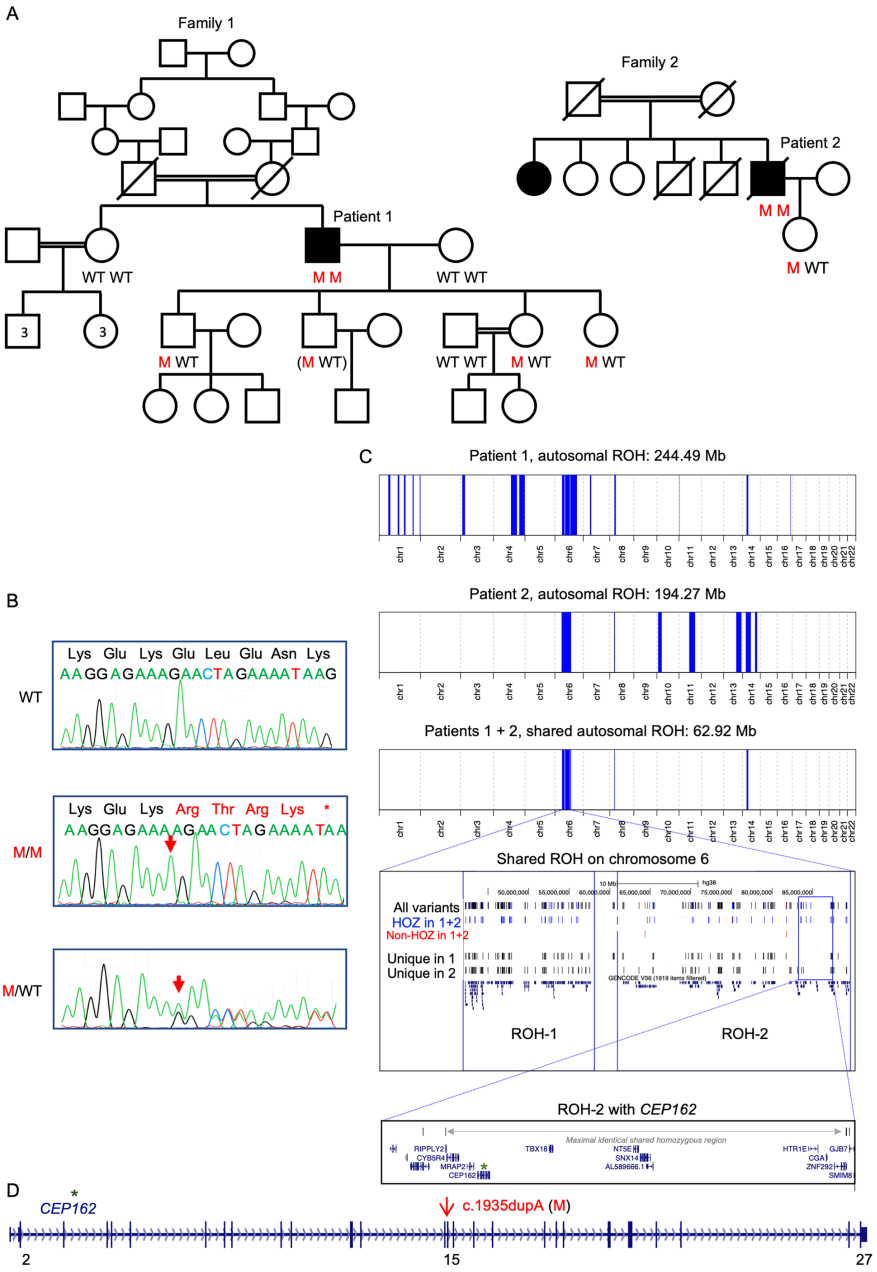

Figure 2-2 Homozygous CEP162 frameshift variant causes RP in 2 unrelated Moroccan families.

A. *Pedigrees with individuals who were available for genotyping of the c.1935dupA [p.(E646R*5)] in CEP162. M, mutation.* ***B.*** *Electropherograms of an individual with WT sequence (upper panel), patient 1 (middle; homozygous 1-bp insertion with frameshift and premature termination codon), and a heterozygous carrier (bottom; all children of the patients).* ***C.*** *ROH on chromosome 6, comprising CEP162, shared by patient 1 and patient 2.* ***D.*** *Scheme of CEP162 gene (to scale). Vertical bars: exons. The pathogenic variant resides in exon 15.*

Patient 2. His older affected sister, living in North Morocco, was not available for testing. WES in the proband generated 40.6 million reads, with 99.0% of reads mapping to the target sequences, providing an average coverage of >30x. Assessment of 275 RetNet genes did not reveal any (likely) pathogenic variants. An exome-wide analysis

revealed 1,298 rare variants (MAF <1%), 190 of which were homozygous. These were reduced to 58, filtering with ROH (Figure 2-2C), and ultimately to the *CEP162* c.1935dupA variant, based on the aforementioned criteria.

Patient 1 & 2. Segregation analysis in both families supported a pathogenic nature of the truncating *CEP162* variant (Figure 2-2A, B) which was absent from gnomAD (v.2.1.1). No homozygous *CEP162* LoF variants were found in gnomAD. The variant was neither found in 70 RP patients from North Africa (incl. 43 from Morocco) by targeted testing, nor in WES data from 1,184 IRD cases. The largest ROH in both Patient 1 and 2 is located on chromosome 6 (Figure 2-2C) and includes the *CEP162*: c.1935dupA variant, putting it forward as a potential founder allele (Figure 2-2C**)**.

2.3.3 Mutated c.1935dupA CEP162 mRNA escapes nonsense-mediated decay in patient fibroblasts, allowing for expression of truncated CEP162 protein

Fibroblasts from Patient 1 were compared to control human dermal fibroblasts. qRT-PCR analysis revealed that *CEP162* transcript levels were significantly reduced in patient fibroblasts **(**Figure 2-3A**).** *CEP162* mRNA levels significantly increased upon serum starvation, suggesting that the transcriptional regulation of the *CEP162* gene remained unaffected (Figure 2-3A). Anisomycin treatment was used to determine whether the patient *CEP162* transcript undergoes nonsense-mediated decay (NMD). Increased expression of *CEP162* after anisomycin treatment was observed in both patient and control cells (Figure 2-3B), suggesting that a basal level of *CEP162* transcript physiologically undergoes NMD.

To determine whether the truncated CEP162-E646R*5 protein is expressed in patient fibroblasts, we immunoblotted control and patient fibroblast lysates with an

antibody that recognizes the N-terminus of CEP162 prior to the truncation. Patient lysates only had a band at the predicted size of truncated CEP162 (~75 kDa) compared the full-length CEP162 (~160 kDa) band in control lysates (Figure 2-3C). In addition, probing with the C-terminus anti-CEP162 antibody produced a full-length CEP162 band in control lysate, but no corresponding or truncated band in the patient lysate (Figure 2-3C). We conclude that despite the lower levels of *CEP162* mRNA, the residual transcript does not undergo complete NMD, resulting in expression of truncated CEP162-E646R*5 protein in patient cells (Figure 2-3D).

*2.3.4 CEP162-E646R*5 mutant protein binds microtubules but is unable to associate with centrioles or CEP290*

Human CEP162 comprises 1,403 amino acids with 3 CC stretches in its C-terminus: CC1 (residues 617-906), CC2 (957-1,121) and CC3 (1,167-1,386). CEP162 associates with microtubules through its CC1/CC2 domains and with centrioles through its CC3 domain[149]. The c.1935dupA mutation results in early truncation of the protein after the first 29 amino acids of the CC1 domain (Figure 2-4A). Truncated FLAG-CEP162-E646R*5 produced a ~80 kDa band compared to the full-length FLAG-CEP162 band at ~165 kDa (Figure 2-4B, Figure 2-6A). We performed a microtubule binding assay to determine whether the CEP162-E646R*5 mutant protein binds microtubules. Immunoprecipitated FLAG-tagged human CEP162 full-length or E646R*5 mutant protein were co-pelleted with taxol-stabilized microtubules. Figure 2-4C shows both full length FLAG-CEP162 and

truncated FLAG-CEP162-E646R*5 were found in the microtubule pellets suggesting that the residual CC1 domain is sufficient to bind microtubules.

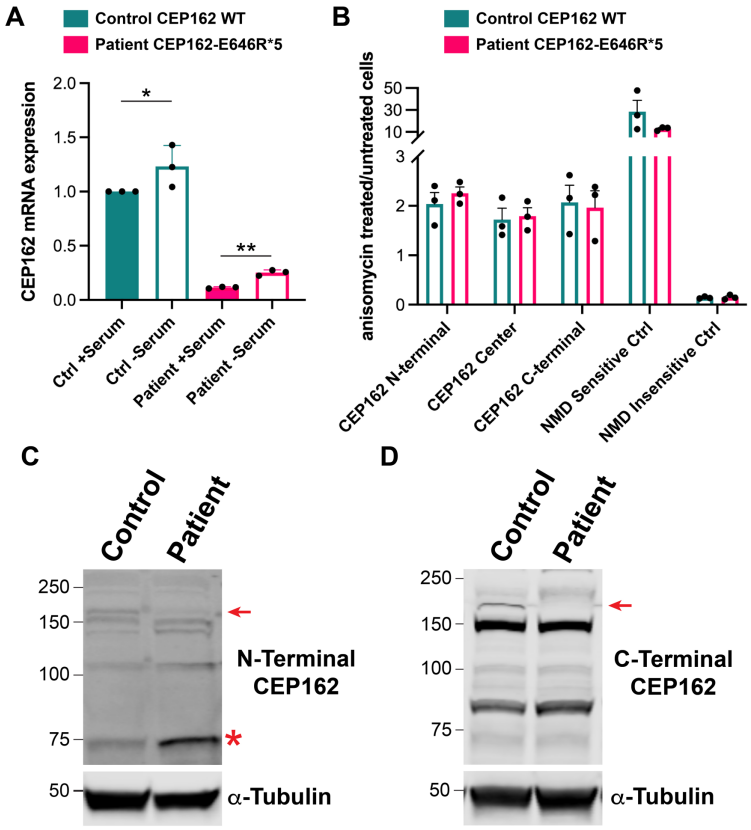

Figure 2-3 CEP162 mRNA expression is reduced, but truncated CEP162-E646R*5 protein is expressed in patient fibroblasts.

A *Transcript levels of CEP162 in control and patient fibroblasts after 24 hours +/– serum conditions. Quantitative RT-PCR using primer sets across exons 5, 14 and 25 of the CEP162 gene was performed in triplicate from three biological replicates at each condition. We found the Ct value between each primer set was consistent providing high confidence that the entire CEP162 mRNA was reverse transcribed. Therefore, the relative mRNA expression level in each sample was calculated by taking an average of the Ct values for all primer sets normalized to the housekeeping gene HSP90. Error bars represent SD. An ordinary one-way ANOVA was performed, +/– Ctrl serum $^{ns}p=0.1553$, +/– Patient serum $^{ns}p=0.6743$, Ctrl vs Patient + serum **p=0.0065, Ctrl vs Patient – serum **p=0.0016.* ***B*** *Inhibition of NMD by anisomycin treatment results in a similar increase in fibroblasts of patient and controls. Bar and scatter plot of three independent experiments analyzed in duplicates by ddPCR.* ***C-D*** *Representative Western blot of control and patient fibroblast lysates. Blots were probed with an N-terminal anti-CEP162 antibody to detect full length (red arrow) and truncated (red asterisk) bands (**C**). C-terminal anti-CEP162 antibody only detected full length CEP162 (red arrow) in the control fibroblast lysates. α-tubulin was used as a loading control.*

To determine whether this truncated mutant protein associates with the centrioles, we co-transfected the FLAG-tagged CEP162 constructs with the ciliary marker Htr6-GFP into IMCD3 cells and serum-starved for 24 hours to ciliate the cells (Figure 2-4D). Full-

length FLAG-CEP162 was present at the basal bodies of Htr6-GFP-positive cilia where it co-localizes with γ-tubulin. In addition, co-staining with a proximal-end centriole protein, CEP250, showed proper localization of FLAG-CEP162 to the distal end of the centrioles. In contrast, the mutant FLAG-CEP162-E646R*5 was not detected at the basal body (Figure 2-4D).

It was previously shown that CEP162 interacts with CEP290 through its CC1/CC2 domain[149]. To determine whether the mutant CEP162-E646R*5 protein interacts with endogenous CEP290, we performed FLAG immunoprecipitations from our transfected 293T cells expressing either full length or mutant CEP162. FLAG-CEP162-E646R*5 was unable to pull down CEP290; however, CEP290 localization at the centrioles was normal

in the patient fibroblasts (Figure 2-4E, F). Also, no difference in CEP290 protein levels was observed in patient fibroblasts compared to controls (Figure 2-8)

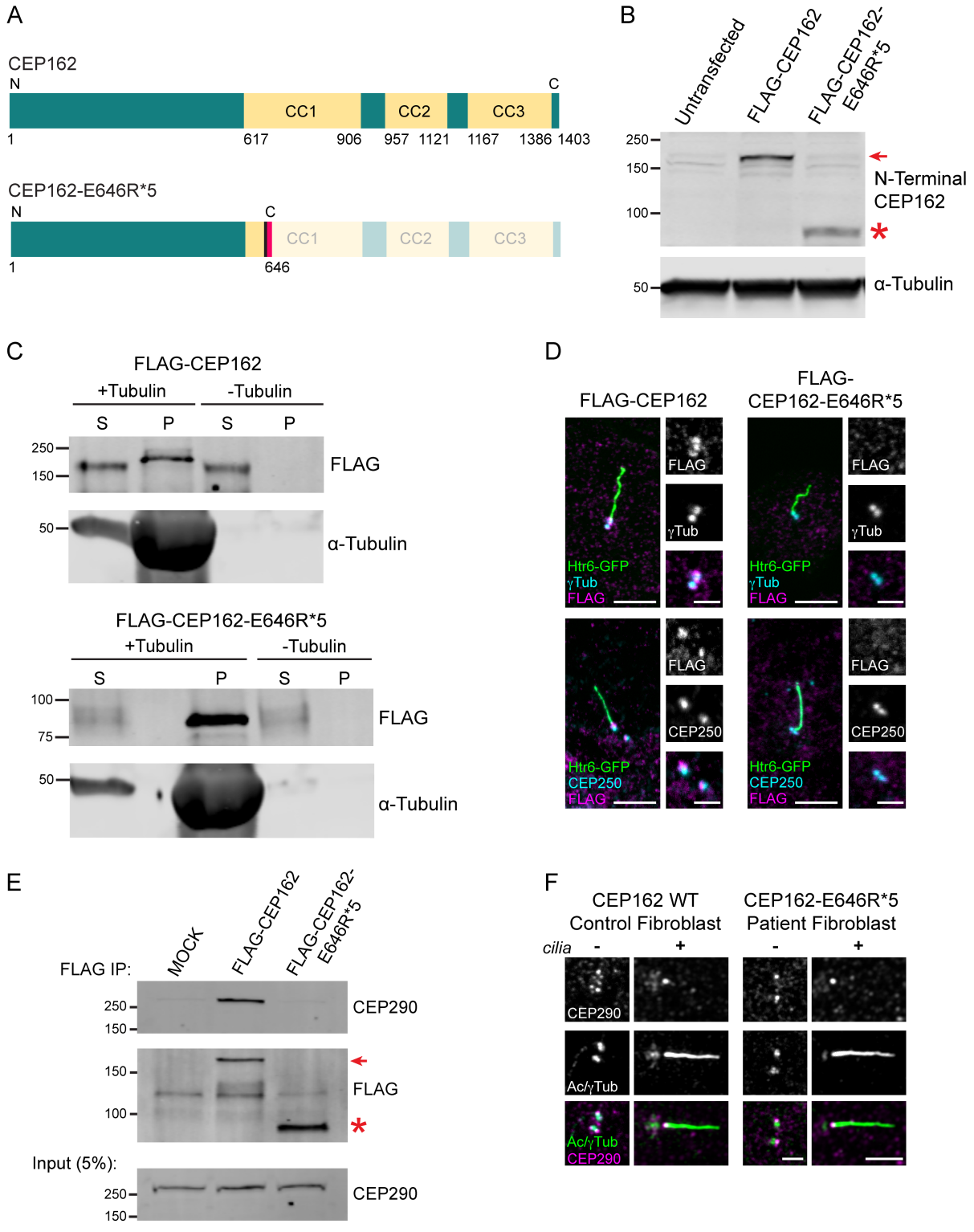

Figure 2-4 Effect of E646R*5 mutation on CEP162 protein expression and localization.

***A**. Scheme of human CEP162 protein with 3 C-terminal coiled-coil (CC) domains and the truncated CEP162-E646R*5 mutant protein. The amino acid residues are given for each scheme. **B** Western blot of 239T cell lysates from untransfected control, transfected FLAG-CEP162 (~165 kDa, red arrow) and FLAG-CEP162-E646R*5 (~80 kDa, red asterisk). Blots were probed for CEP162 to detect expressed protein and α-tubulin as a loading control. **C** Microtubule binding assay. Purified FLAG-CEP162 or FLAG-CEP16-E646R*5 was co-pelleted with taxol-stabilized microtubules. CEP162 was probed by anti-FLAG antibodies and pelleted microtubules were detected by anti-αTubulin antibodies. S, supernatant; P, pellet. **D** Serum-starved IMCD3 cells co-expressing Htr6-GFP and FLAG-CEP162 or FLAG-CEP162-E646R*5. Transfected cells were identified by GFP (green) fluorescence in the cilium. FLAG (magenta) was co-immunostained with either γ-tubulin (cyan, basal bodies) or CEP250 (cyan, proximal-end centriolar protein). **E** FLAG immunoprecipitation from Mock, FLAG-CEP162 or FLAG-CEP162-E646R*5 transfected 293T cells lysates. Endogenous CEP290 pulls down with full length FLAG-CEP162, but not MOCK or FLAG-CEP162-E646R*5. **F** CEP290 (magenta) immunostaining in control and patient fibroblasts co-stained with γ-tubulin (green). Higher magnification images of the cilium/basal body and corresponding staining are shown to the right. Scale bars, 5 μm and 2 μm.*

2.3.5 Patient fibroblasts have delayed ciliation

CEP162 is present at the centrioles throughout the cell cycle, and its microtubule-binding activity is believed to direct its localization to the mitotic spindle during cell division[149]. Patient fibroblasts expressing the CEP162-E646R*5 truncated protein had a normal growth rate and no aneuploidy was detected in 30 metaphases. Consistent with our result showing that microtubule binding is retained by truncated CEP162-E646R*5, CEP162 staining decorated the microtubule spindles of dividing cells in the patient fibroblasts similar to controls (Figure 2-5A). This result suggests that truncated CEP162-E646R*5 localization and function is normal during fibroblast mitosis, which is expected since CEP162's role in post-mitotic quiescence has only been described for neurons[146,148].

As for ciliary localization, we found that CEP162 co-localizes with γ-tubulin-positive centrioles in control fibroblasts but was not detected in patient fibroblasts (Figure 2-5B). While control fibroblasts produced cilia within 24 hours, very few cilia in patient fibroblasts were observed before 72 hours of serum withdrawal (Figure 2-5C). We used correlative light and scanning-electron microscopy (CLSEM) to examine the structure of the arrested cilia in the patient fibroblasts and compared them to normal cilia produced in control

fibroblast. While control fibroblasts had Arl13b-positive primary cilia, patient fibroblasts only produced Arl13b-positive blebs on their surface (Figure 2-5D). Additionally, polyglutamylated tubulin staining was not observed in the stalled patient cilia indicating ciliogenesis is halted prior to axoneme extension in patient fibroblasts (Figure 2-6B, C). Together, this suggests that the ciliary membrane has fused with the plasma membrane, resulting in a bulbous bleb on the cell's surface.

By 72 hours after serum withdrawal, the number of cilia produced in the patient fibroblasts were not significantly different from those produced in the control fibroblasts (Figure 2-5C). Ciliary length was measured for every cilium imaged at the 3 timepoints. At 72 hours, the patient cilia were significantly longer than the control cilia ($p>0.0001$, Figure 2-5E, F). Together, our data suggest that in patient fibroblasts, ciliogenesis is paused before axoneme extension, but these cells can ultimately overcome the loss of CEP162 at the centrioles and produce cilia. Accumulation of ciliary membrane before axoneme elongation could affect the final length of the cilium in the patient fibroblasts.

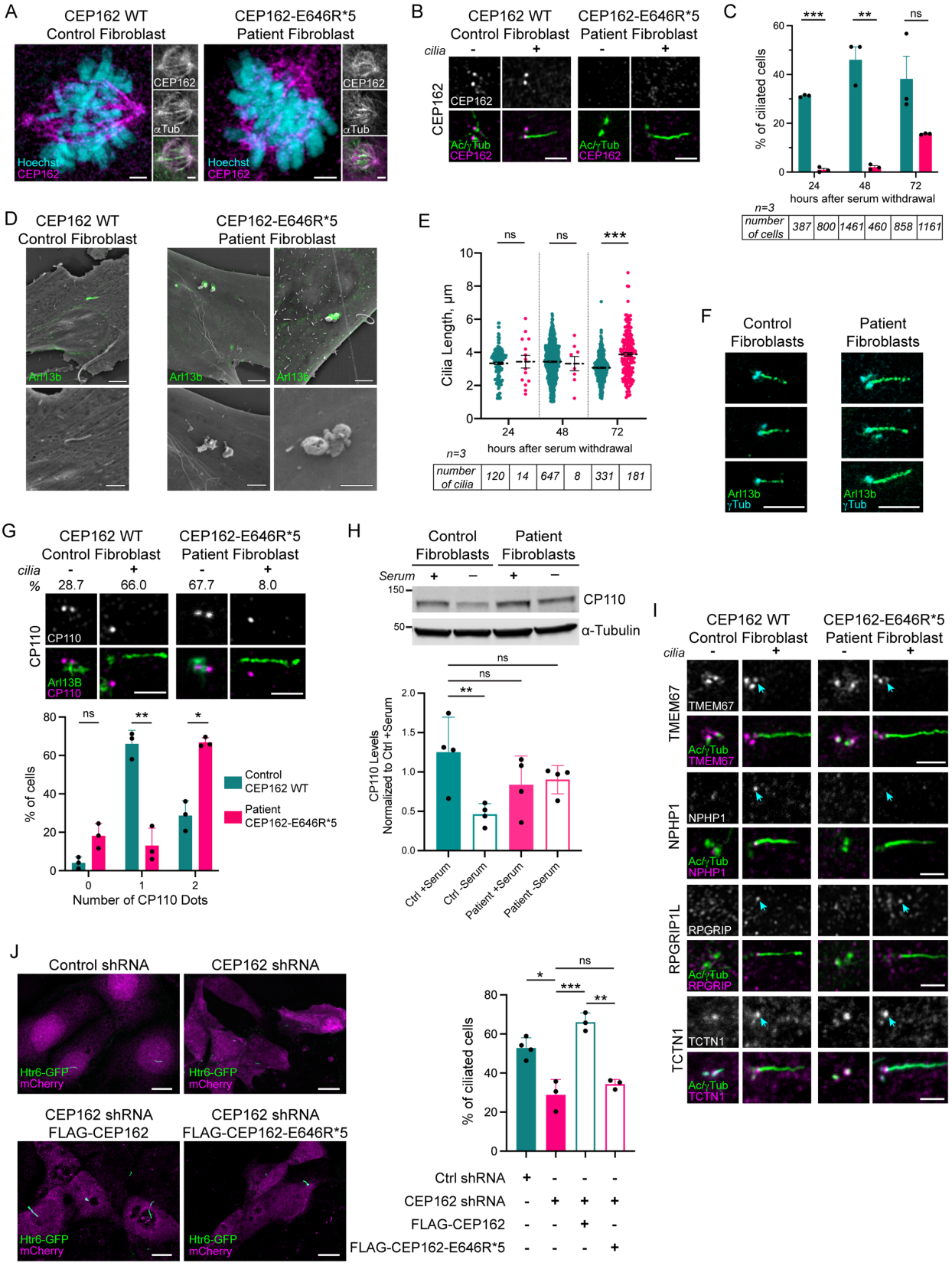
A
CEP162 WT
Control Fibroblast
CEP162-E646R*5
Patient Fibroblast
CEP162
αTub
Hoechst
CEP162
B
CEP162 WT
Control Fibroblast
CEP162-E646R*5
Patient Fibroblast
cilia
CEP162
Ac/γTub
CEP162
C
% of ciliated cells
hours after serum withdrawal
n=3
number of cells
387
800
1461
460
858
1161
D
CEP162 WT
Control Fibroblast
CEP162-E646R*5
Patient Fibroblast
Arl13b
E
Cilia Length, µm
hours after serum withdrawal
n=3
number of cilia
120
14
647
8
331
181
F
Control Fibroblasts
Patient Fibroblasts
Arl13b
γTub
G
CEP162 WT
Control Fibroblast
CEP162-E646R*5
Patient Fibroblast
cilia
%
28.7
66.0
67.7
8.0
CP110
Arl13B
CP110
% of cells
Control
CEP162 WT
Patient
CEP162-E646R*5
Number of CP110 Dots
H
Control
Fibroblasts
Patient
Fibroblasts
Serum
CP110
α-Tubulin
CP110 Levels
Normalized to Ctrl +Serum
Ctrl +Serum
Ctrl -Serum
Patient +Serum
Patient -Serum
I
CEP162 WT
Control Fibroblast
CEP162-E646R*5
Patient Fibroblast
cilia
TMEM67
Ac/γTub
TMEM67
NPHP1
Ac/γTub
NPHP1
RPGRIP1L
RPGRIP
Ac/γTub
RPGRIP
TCTN1
Ac/γTub
TCTN1
J
Control shRNA
CEP162 shRNA
Htr6-GFP
mCherry
CEP162 shRNA
FLAG-CEP162
CEP162 shRNA
FLAG-CEP162-E646R*5
% of ciliated cells
Ctrl shRNA
CEP162 shRNA
FLAG-CEP162
FLAG-CEP162-E646R*5

Figure 2-5 CEP162-E646R*5 localizes to the mitotic spindle in patient fibroblasts, but its absence from the basal body delays ciliation.

A *Control and patient fibroblasts co-stained for endogenous CEP162 (magenta) and α-tubulin show CEP162-E646R*5 protein at the mitotic spindle. Individual staining is shown to the right. Scale bars 2 μm.* ***B*** *CEP162 (magenta) immunostaining in control and patient fibroblasts co-stained with acetylated/γ-tubulin (Acetyl/γTub, green). Scale bar, 2 μm.* ***C*** *Percent ciliation in control and patient fibroblasts after 24, 48 or 72 hours after serum withdrawal was determined by Arl13b and γ-tubulin staining. ***p<0.000001, **p<0.001* ***D*** *Correlative light and scanning electron microscopy were performed in control and patient fibroblasts. Cilia were identified by staining for Arl13b (green). Merged images are shown for the low scanning electron micrograph with magnified micrographs shown below. Scale bars, 4 μm and 2 μm.* ***E*** *Cilia length was measured for each cilium. ***p<0.0001* ***F*** *Representative cilia from control and patient fibroblasts stained with Arl13b (green) and γ-tubulin (cyan). Scale bar, 5 μm.* ***G*** *Immunostaining of CP110 (magenta) in control and patient fibroblasts, with (+) and without (-) cilia. Percent observed below. Bar graph quantifying CP110 dots in control and patient fibroblasts.* ***H*** *Representative Western blot from control and patient fibroblast lysates after 24 hours with (+) or without (–) serum. Blots were probed for CP110 and α-tubulin for a loading control. Bar graph quantifying relative levels of CP110 in control and patient fibroblasts +/– serum from 4 independent experiments. *p<0.035* ***I*** *Immunostaining of transition zone proteins TMEM67, RPGRIP1L, NPHP1 and TCTN1 (magenta) in control and patient fibroblasts, +/– cilia. In all panels, cilia/basal bodies were co-stained with acetylated/γ-tubulin (Acetyl/γTub, green), and cyan arrows mark transition zone. Scale bars, 2 μm.* ***J*** *Representative immunofluorescence images showing cilia (Htr6-GFP, green) in control or CEP162 shRNA targeted cells (mCherry, magenta) as well as CEP162 shRNA targeted cells co-expressing either full-length FLAG-CEP162 or FLAG-CEP162-E646R*5. Scale bars, 10 μm.* ***K****. Bar graph shows percent ciliation in control or CEP162 shRNA expressing IMCD3 cells. Ciliation was rescued by expression of the full-length FLAG-CEP162, but not FLAG-CEP162-E646R*5. *p<0.019, **p<0.0019*

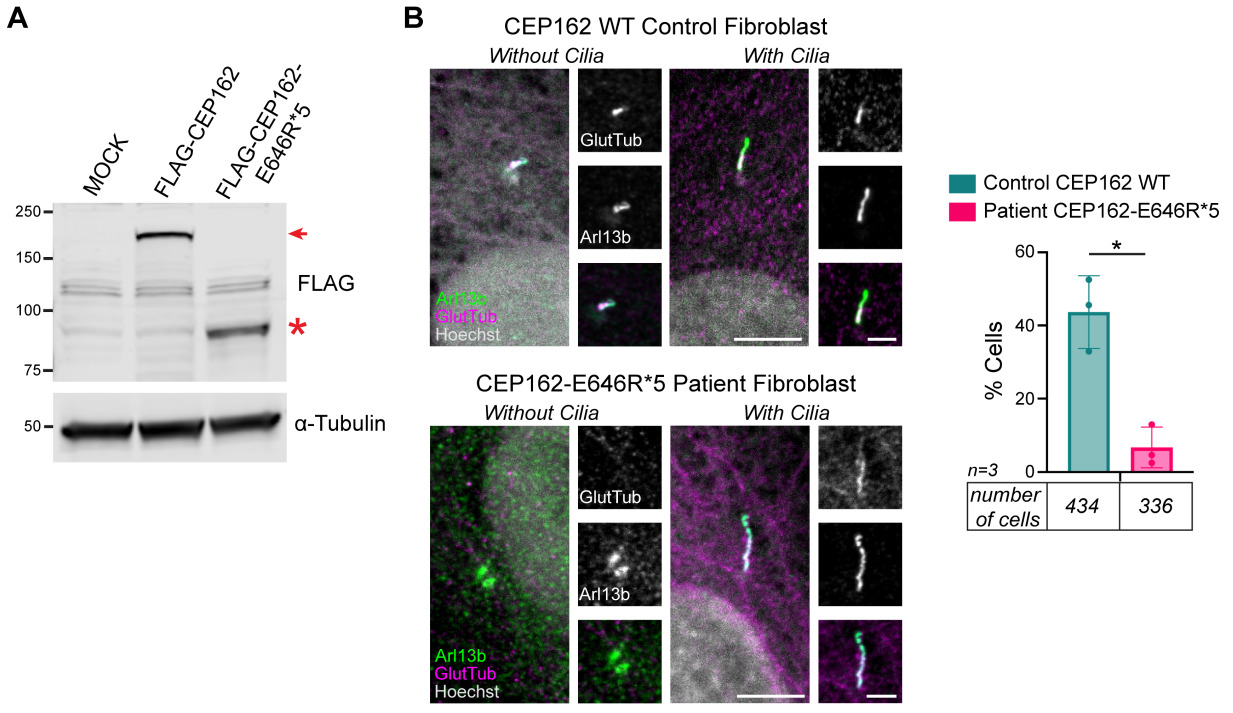

Figure 2-6 FLAG-CEP162 and FLAG-CEP162-E646R*5 expression in 293T cells and glutamylated tubulin staining in control and patient fibroblasts.

A *Representative Western blot of 239T cell lysates from untransfected control, FLAG-CEP162 (~165 kDa, red arrow) and FLAG-CEP162-E646R*5 (~80 kDa, red asterisk). Blots were probed for FLAG to detect expressed protein as well as α-tubulin as a loading control.* ***B*** *Control and patient fibroblasts with and without a cilium were co-stained with Arl13b and glutamylated tubulin B3 (GlutTub, magenta). Nuclei labeled with Hoechst 33342 (grey). Scale bars, 5 μm and 2 μm.* ***C.*** *Bar graph quantifying the % of control or patient fibroblasts with positive glutamylated tubulin staining shown on the right. A Welch's two-tailed t test was performed, *p=0.011. Error bars represent SD.*

2.3.6 Persistence of CP110 at the mother centriole delays primary ciliogenesis in patient fibroblasts

To determine the stage at which ciliogenesis is paused in patient fibroblasts, we analyzed the localization of molecular components involved in cilia formation. First, maturation of the basal body appears to be normal, as proteins involved in ciliary vesicle fusion (EHD1), DA formation (CEP164) and IFT machinery recruitment (IFT88) were normal (Figure 2-7A). Following ciliary vesicle formation, CP110, a distal-end centriole protein that prevents microtubule nucleation, is removed from the mother centriole, and degraded to enable proper axoneme elongation[77]. This regulatory step was previously reported to be unaffected by loss of CEP162 in RPE1 cells[149]. In patient fibroblasts, however, quantification of CP110 dots revealed persistence of CP110 at the mother centriole of stalled cilia after 48 hours of serum withdrawal (Figure 2-5G). In addition, Western blot analysis for CP110 indicates that while levels normally decrease 50% upon serum starvation in controls, levels of CP110 remained unchanged in the patient fibroblasts 24 hours after serum withdrawal (Figure 2-5H; Figure 2-8). CP110 removal is controlled by CEP164-mediated recruitment of the serine/threonine protein kinase, TTBK2, to the distal appendages[75,155]. TTBK2 phosphorylates multiple targets, such as CEP83 and MPP9, that are required for CP110 removal and ciliogenesis[77,156]. We found

both TTBK2 and its MPP9 substrate were normally localized in the patient fibroblasts (Figure 2-7B). Although the molecules needed to remove CP110 from the mother centriole are present, this process is delayed by the loss of CEP162 at the basal body.

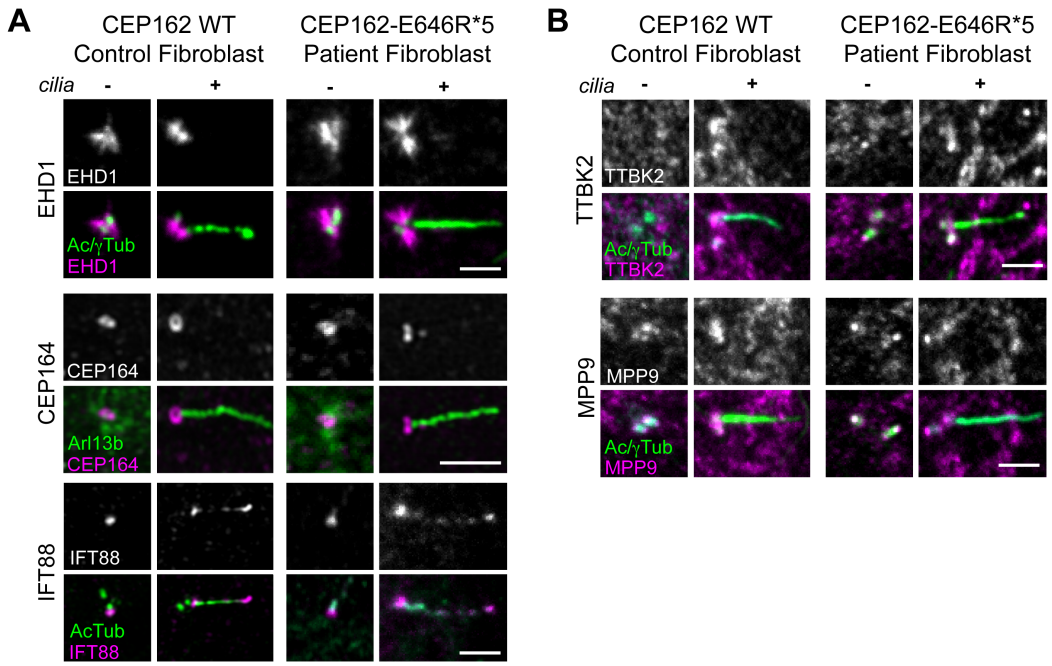

Figure 2-7 Immunostaining for proteins implicated in early stages of TTBK2 and MPP9 in control and patient fibroblasts.

A. *Immunostaining of early ciliogenesis markers in control and patient fibroblasts: EDH1, CEP164, and IFT88 (magenta).* ***B.*** *Molecules implicated in the removal of CP110: TTBK2 and MPP9 (magenta) are normally localized at the basal body of patient fibroblasts.*

It was reported by Wang *et al.*[149] that exogenous expression of a C-terminally truncated CEP162, which maintains microtubule association but is unable to localize to centrioles, resulted in cilia that were abnormally long. In these experiments, C-terminally truncated CEP162 was found at the axoneme tip of elongated cilia where it ectopically recruited TZ components[149]. Our data show that E646R*5-truncated CEP162 maintains microtubule binding during mitosis but is not localized to centrioles, suggesting it may

behave similarly. To test this, we stained control and patient fibroblasts for 4 TZ proteins: TMEM67, NPHP1, RPGRIP1L, and TCTN1 (Figure 2-5I). We found normal localization of TCTN1, but TMEM67, NPHP1 and RPGRIP1L were not properly assembled at the ciliary base of patient fibroblasts, consistent with the complete loss of CEP162[149]. Importantly, we did not find mislocalization of any of these TZ components to the tip of the long patient cilia (Figure 2-5I), indicating that the CEP162-E646R*5 protein has lost its ability to recruit TZ proteins to cilia.

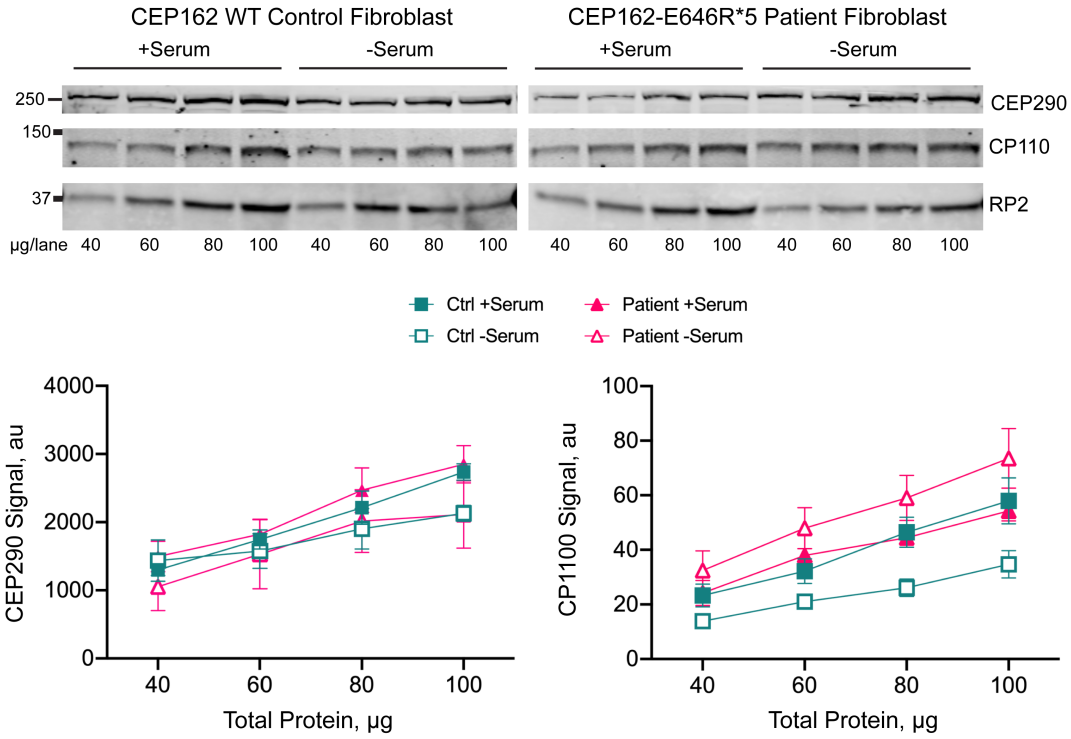

Figure 2-8 Quantification of CEP290, CP110 and RP2 protein levels in CEP162-mutant patient fibroblasts compared to controls.

*Representative Western blots show serial dilutions of control (CEP162-WT) fibroblast and patient (CEP162-E646R*5) fibroblast lysates for CEP290, CP110 and RP2 proteins. Amount of protein lysate (µg) loaded in each lane is displayed below. The fluorescent signal produced by the CEP290 or CP110 bands in three separate experiments was plotted versus total protein loaded. The slope of the curves was used to calculate the amount of each protein in control and patient fibroblasts.*

To confirm that CEP162-E646R*5 had no ciliary function, we performed shRNA knockdown of *CEP162* in IMCD3 cells, followed by rescue with either FLAG-tagged full-length CEP162 or CEP162-E646R*5. A single plasmid co-expressing shRNA and soluble mCherry was used to identify transfected cells and were co-transfected with an Htr6-GFP plasmid to label the cilia. Figure 2-5J shows images of the cilia in mCherry-positive cells when expressing the control or *CEP162* shRNA. *CEP162* knockdown resulted in reduced ciliation compared to control shRNA, similar to previous results[149]. Expression of the FLAG-tagged full-length CEP162 rescued the loss of cilia due to *CEP162* knockdown; however, FLAG-CEP162-E646R*5 was unable to rescue (Figure 2-5J, K). These results support that expression of CEP162-E646R*5 protein does not retain any ciliary function.

2.3.7 CEP162 is expressed in human retina and localizes to the basal body in mouse photoreceptors

We examined *CEP162* expression in single-cell transcriptional data of human neural retina[157]. This revealed high expression in all retinal cell types, especially in ganglion cells (Figure 2-9A). Immunostaining for CEP162 on human retinal sections shows expression throughout the human retina (Figure 2-9B-F), similar to expression previously determined in chick retina[146]. CEP162 is a centriolar protein; to determine its precise localization in photoreceptors, we used Cetn2-GFP transgenic mice that have fluorescently labelled centrioles[158]. In photoreceptors, mother and daughter centrioles form 2 adjacent GFP dots, and the connecting cilium emerges as a GFP streak from the mother centriole. CEP162 staining is localized to the distal end of both mother and daughter centrioles (Figure 2-10A). Airyscan mages were acquired to determine the precise localization of CEP162 in relation to several ciliary markers: Acetylated tubulin for the axoneme,

CEP290 for the connecting cilium, CEP164 for the distal appendages, and CP110 for the daughter centriole (Figure 2-10B). CEP162 decorates the distal ends of each centriole at the base of the photoreceptor outer segment in wild-type mouse retinas.

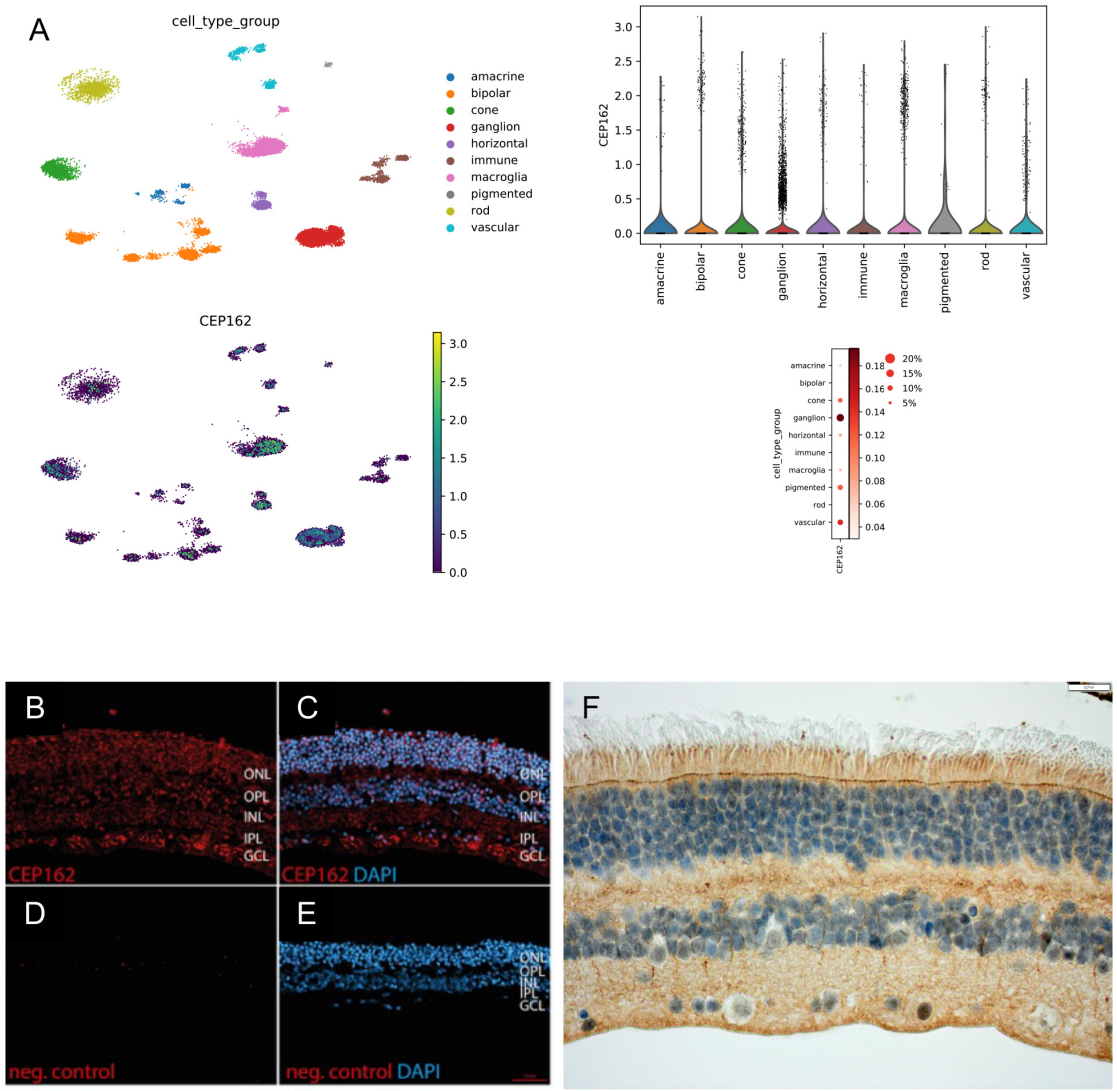

Figure 2-10 Expression analysis of CEP162.

A. *Mining of single-cell transcriptional retinal data displaying the highest expression in cells belonging to the ganglion cell population. (Left) UMAP plot of 19,768 human neural retinal cells colored based on cell type. Visualization of scaled and corrected expression on UMAP plot for CEP162. (Top right) Violin plot for visualization of scaled and corrected expression of CEP162 in the 9,768 human neural retinal cells. (Bottom right) Individual dots are colored and sized to visualize both the proportion of cells in each population expressing a given gene (dot diameter size) and the average expression level of that gene (dot color intensity) in the detected cells.* ***B-F*** *CEP162 immunostaining on human retinal sections. Representative fluorescence images of human paraffin-embedded sections stained with anti-CEP162 antibody (red) (**B-C**) or negative control (**D-E**). Sections were counter-stained with DAPI (blue), displayed in **C** and **E**. Scale bars represent 100 mm.* ***F*** *Immunostaining of the CEP162 protein on human retina is visible in light brown, displaying retinal expression. Light microscopy at 400x. Scale bars represent 100 mm. Abbreviations: GCL, ganglion cell layer; INL, inner nuclear layer; IPL, inner plexiform layer; OPL, outer plexiform layer; ONL, outer nuclear layer; OLM, outer limiting membrane; PR, photoreceptors.*

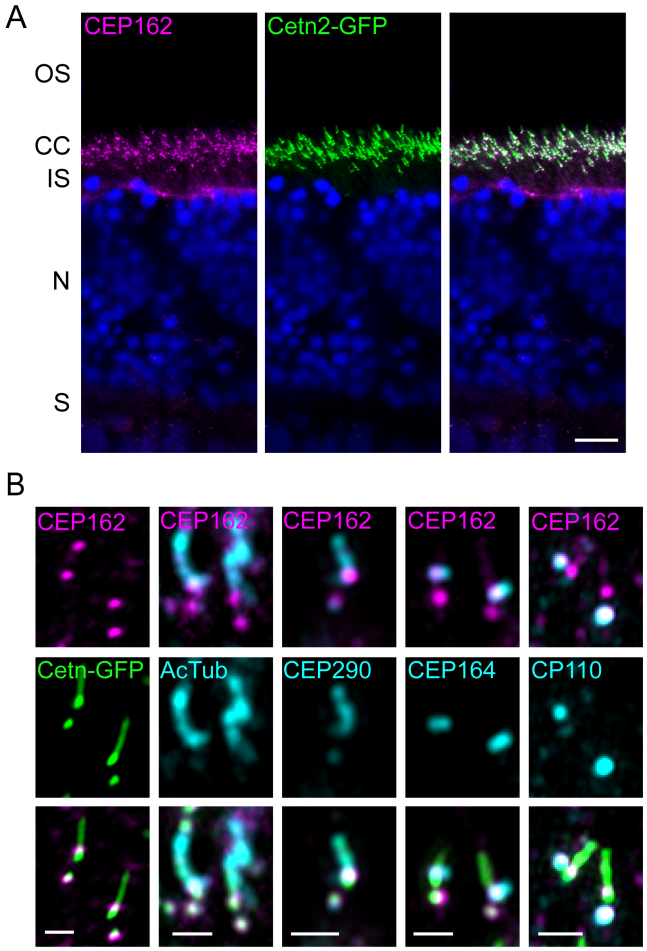

Figure 2-9 Endogenous CEP162 is localized to the distal-end of centrioles at the base of the photoreceptor outer segment in adult wild-type mouse retina.

A. *CEP162 is localized at the photoreceptor connecting cilium, which is marked by GFP fluorescence (green). Scale bar, 10 µm.* ***B*** *High-resolution Airyscan images: CEP162 (magenta) staining decorates the distal ends of each centriole of the basal body at the base of the connecting cilium (Cetn2-GFP, green). Additional Airyscan images of CEP162 counterstained with multiple ciliary markers: Acetylated Tubulin (AcTub), CEP290, CEP164, and CP110 (cyan). Scale bar, 1 µm.*

*2.3.8 CEP162-E646R*5 is unable to localize to the basal body in mouse photoreceptors but can rescue neuronal cell death*

To determine the localization of truncated CEP162-E646R*5 mutant protein in photoreceptors, we employed *in vivo* electroporation[159] to express FLAG-tagged full-length and E646R*5-mutant *CEP162* constructs in mouse rods. We co-expressed Rho-mCherry to label the outer segment in transfected rods and stained retinas with anti-Centrin1 antibodies to label the connecting cilium in all photoreceptors. Figure 2-11A shows that FLAG-CEP162 was primarily localized to the basal body but also found within the connecting cilium in rods with Rho-mCherry-labeled outer segments. The presence of FLAG-CEP162 within the connecting cilium is likely an overexpression artifact but could also be due to epitope masking of endogenous CEP162 within the connecting cilium. In contrast, FLAG-CEP162-E646R*5-mutant staining does not localize to the basal body of Rho-mCherry-labeled outer segments (Figure 2-11B). This suggests that the truncated CEP162-E646R*5-mutant protein is unable to properly localize to the centrioles in photoreceptors.

Using a retroviral antisense knockdown strategy in developing chick eyes, CEP162 (aka QN1) was reported to play a key role in differentiation of retinal neurons[146]. We found that CEP162-E646R*5 maintains microtubule binding at the mitotic spindle in fibroblasts, so it could possibly function in neuronal development. To test this, we *in vivo*-electroporated *CEP162* shRNAs during retinal development and rescued with full-length or truncated *CEP162* constructs. Figure 6C shows representative retinal sections from P15 mice expressing a single plasmid co-expressing control or *CEP162* shRNA and soluble mCherry to identify electroporated rods. Pycnotic nuclei were counted within each

electroporated area and normalized to the number of mCherry positive rods. Knockdown of *CEP162* increased cell death ~4-fold compared to controls, which was rescued by expression of either full-length or CEP162-E646R*5 (Figure 2-11C).

In conclusion, our data suggest that CEP162-E646R*5 retains microtubule binding at the mitotic spindle that allows it to function during neuroretina development, yet its absence from the ciliary basal body limits recruitment of a few TZ proteins likely underlying late-onset RP in both patients.

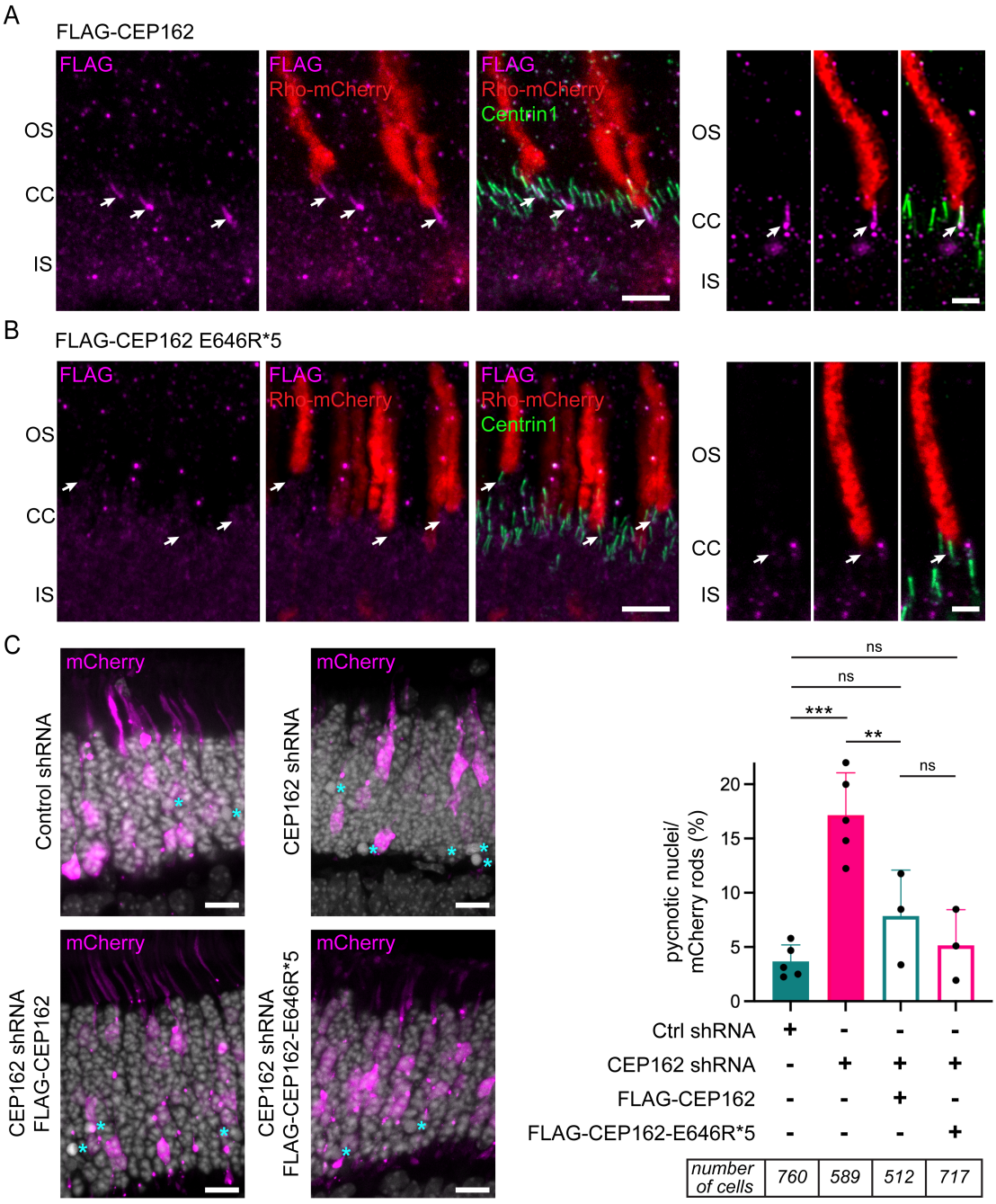

Figure 2-11 CEP162-E646R*5 mutant protein does not localize to centrioles in adult mouse rod photoreceptors but does participate in retinal neurogenesis.

A-B *Wild-type mouse rods were transfected with FLAG-CEP162 (**A**) or FLAG-CEP162-E646R*5 (**B**, magenta) and rhodopsin-mCherry (red) as a transfection marker. Centrin1 (green) immunostaining was conducted to label the connecting cilium. Arrows indicate the basal body of the transfected rods. Scale bars, 5 µm and 2 µm.* ***C*** *Developing mouse retina (P0-P1) were electroporated with control or CEP162 shRNA plasmids co-expressing a soluble mCherry (magenta), and CEP162 knockdown was rescued with either FLAG-CEP162 or FLAG-CEP162-E646R*5. Scale bar, 5 µm. Cell death was assessed by counting pycnotic nuclei labeled with DAPI (grey, cyan asterisk) and quantified for a minimum of 3 separate animals. ***p<0.0007, **p<0.0054, *p<0.036.*

2.4 Discussion

Human ciliopathies are a diverse group of syndromic and non-syndromic diseases that involve several organ systems as cilia are ubiquitous cellular organelles[160]. Understanding how ciliary genes act in a tissue-specific manner to produce the wide variety of human phenotypes remains an active area of study. Here, we identified a homozygous frameshift variant in RP patients from 2 unrelated families. We find that *CEP162* is expressed in human retina and localizes to the basal body of outer segments in mice photoreceptors, and we provide strong functional evidence that *CEP162* plays a dual role in the retina.

In patient fibroblasts, low levels of *CEP162* mRNA were preserved and sufficient to produce an – albeit heavily truncated – CEP162 protein. We show that the residual truncated CEP162 protein maintains microtubule binding and is present at the mitotic spindles in patient-derived fibroblasts. These cells also had a normal complement of chromosomes and growth rates, consistent with previous knockdown *of CEP162* in RPE1 cells[149]. CEP162's role in cell division was previously attributed to post-mitotic arrest of retinal neurons[146,148]. We found that knockdown of *CEP162* in developing mouse retina increased neuronal cell death, which was rescued by expression of not only the full-length, but also truncated CEP162. This suggests that the truncated CEP162-E646R*5 protein retains function in neuroretina development likely due to its preserved microtubule binding activity. Mutations that disrupt CEP162 microtubule binding would likely result in defective retinal neurogenesis.

In quiescent cells, CEP162 is known to play a functional role in ciliogenesis by promoting TZ assembly[149]. Truncated CEP162-E646R*5 protein was unable to localize

to the ciliary basal body. The loss of CEP162 from the cilia results in reduced recruitment of some TZ proteins to cilia in patient fibroblasts. We confirm through rescue experiments that the truncated CEP162 is unable to restore the loss-of-function phenotype at the cilium. In the patient fibroblasts, we found that cilia formation was delayed due to the persistence of CP110 at the mother centriole. CP110 caps the distal end of centrioles, and its removal and degradation are prerequisites for ciliation. Other aspects of early ciliogenesis, like the acquisition of distal appendages and fusion of the ciliary vesicle to the plasma membrane, were unaffected in patient's fibroblasts. Interestingly, after extended serum starvation, there was a dramatic increase in generation of – although abnormally long – cilia, showing that ciliogenesis does occur in the absence of CEP162.

It is interesting to speculate that perhaps the retinal defect in the patient (with residual CEP162 neurogenesis function) is not due to impaired ciliogenesis *per se*, as we find that cilia can still be formed, but instead due to reduced recruitment of TZ proteins, such as NPHP1, to the photoreceptor cilium. This could result in structural defects that are particularly detrimental to the outer segment, impairing photoreceptor *maintenance* rather than *formation* – clinically manifesting as late-onset RP and not as congenital retinal disease (as in *CEP290*-associated LCA)[161].

In summary, our data uncover a dual role for the centriolar protein, CEP162, in retinal neurons to ensure proper neurogenesis and ciliary TZ assembly. Our genomic, cell-based, and *in vivo* data show that although the mitotic function of CEP162 during neuronal development is maintained, specific loss of CEP162 function at the cilium results in a novel retinal ciliopathy in humans. These findings highlight the tissue-specific roles of ciliary proteins and may be instrumental for future studies exploring diverse ciliopathies.

2.5 Materials and Methods

2.5.1 Clinical assessment

Patients underwent ophthalmologic evaluation, including slit lamp examination, widefield color fundus photography and blue light autofluorescence (CLARUS 500; Carl Zeiss Meditec Inc., Dublin, CA), and spectral domain optical coherence tomography (Spectralis SDOCT, Heidelberg Engineering, Germany; PLEX Elite 9000; Carl Zeiss Meditec Inc.). Abdominal ultrasound (and additional CT in Patient 2) was conducted to exclude cysts of the kidneys and liver fibrosis.

2.5.2 Genetic and genomic studies

Genomic testing. For the index patients of both families, Patients 1 and 2, genomic DNA (gDNA) was extracted from leukocytes, and pooled libraries were paired-end sequenced on an Illumina NextSeq500 (Illumina, San Diego, CA). Nucleotides were numbered with nucleotide ‘A’ of the ATG as ‘c.1’ (HGVS guidelines, http://www.hgvs.org). Maximum minor allele frequency (MAF) cut-off was 1%. Variants were checked for presence in ClinVar and HGMD databases[162,163] and classified based on ACMG and ACGS guidelines[164–167]. Patient 1. Targeted NGS (IDT xGen® Inherited Diseases Panel v1.0; IDT Integrated Technologies, Coralville, IA), WES (IDT xGen® Exome Research Panel v1.0) and variant assessment were conducted as reported previously[168]. After targeted NGS, variant analysis was performed for 204 genes knowingly associated with IRD, including $RPGR_{ORF15}$ (SeqNext module of SeqPilot software, JSI Medical Systems). Genes associated with the Human Phenotype Ontology (HPO) term "Retinal dystrophy" (HP:0000556) were searched for pathogenic homozygous or potentially compound-

heterozygous variants (varSEAK Pilot 2.0.2, JSI Medical Systems). After WES, the CCG pipeline[169] and interface (Varbank 2.0) were used for data analysis as described[170,171]. ExAC and gnomAD databases[172] (as of 02/2021) were searched for candidate variants identified in homozygous state. Patient 2. WES was performed using the SureSelect XT Human All Exon V6 kits (Agilent, Santa Clara, CA, USA). CLC Genomics Workbench version 7.0.5 (CLCBio, Aarhus, Denmark) was used for read mapping against the human genome reference sequence (NCBI, GRCh37/hg19), removal of duplicate reads, coverage analysis, and quality-based variant calling, followed by further variant annotation using Alamut Batch (Interactive Biosoftware, Rouen, France). Variants were scored heterozygous or homozygous and assessed with our in-house variant filtering and visualization tool. 275 RetNet genes were assessed (version 4 of the RetNet panel), followed by assessment of homozygous variants in the exome. Copy number variations (CNVs) were assessed using ExomeDepth (v1.1.10)[173]. Segregation analysis and screening for the CEP162 variant c.1935dupA p.(E646R*5) in IRD patients. Available members of Families 1 and 2 and 70 RP patients from North Africa, including 43 from Morocco, were tested for the CEP162 variant c.1935dupA p.(E646R*5) by Sanger sequencing (primer sequences: Supplemental Table 1). Pseudonymized WES data from 1,184 IRD cases were also analyzed for presence of the variant (Ghent University Hospital).

Run of homozygosity (ROH) detection and haplotype analysis. Patient 1. ROH were identified using HomozygosityMapper applying default settings[174]. ROH <3 kb adjacent to each other were merged manually, reducing ROH from 71 to 67. Patient 2. ROH were initially mapped by genome-wide single-nucleotide polymorphism (SNP) chip

analysis (HumanCytoSNP-12 BeadChip platform, Illumina). ROH (>1 Mb) were identified using PLINK software[175] integrated in ViVar[176] and ranked according to length and number of consecutive homozygous SNPs. Patient 1 and 2. ROHs were determined with AutoMap[177] using VCF files from both patients (hg38). After identification of individual ROH, shared ROH (coordinate-wise) were determined (Figure 2C, Supplemental Table 1). To define the shared ROH on chromosome 6 and the common haplotype containing the CEP162 variant, all WES variants on chromosome 6 were considered, irrespective of their zygosity (Figure 2C).

Fibroblast culture from skin biopsy. Fibroblasts were isolated from a dermal punch biopsy of the upper arm of Patient 1 as described[178]. The skin biopsy was cut in 18-24 equally sized pieces and plated on a 6-well plate coated with 0,1% Gelatin. Fibroblasts migrated out of the skin biopsies after 7-10 days and were split on 2 75 cm^2 flasks after 3-4 weeks. At 90% confluency, the 2 flasks were split on 3 175 cm^2 flasks. After isolation, fibroblasts were routinely cultured in IMDM/Glutamax containing 15% fetal bovine serum (FBS) and 1% penicillin/streptomycin (all Invitrogen, Waltham, MA). Normal Primary Human Dermal Fibroblasts (HDFa, ATCC #PCS-201-012; Gaithersburg, MD) served as controls.

Karyotyping. 30 metaphases from cultured Patient 1 fibroblasts were analyzed (standard procedures).

2.5.3 Mouse studies

Mice protocols were approved by IACUC at the University of Michigan (registry number A3114-01). Albino Cetn2-GFP transgenic mice were obtained from Jackson Labs (Strain # 027967; Bar Harbor, ME). The *Pde6b*^{Rd1} mutation was removed by backcrossing to a

BALB/cJ albino mouse from Jackson Labs. Albino CD-1 wild-type mice were from Charles River (Strain # 022; Mattawan, MI). All mice were housed under a 12/12-hour light cycle. Experimenters were not blinded to genotype.

In vivo electroporation: Retinal transfection of CD-1 neonatal mice was conducted as previously described[159,179,180]. In P0-P2 neonates, 2 μg/μl shRNA and 1 μg/μl rhodopsin-mCherry plasmid DNA was deposited subretinal. Retinal tissue was collected at P20-P22 for protein localization studies and collected at P14-15 for nuclear counts after shRNA knockdown.

2.5.4 In vitro functional studies

DNA constructs. DNA constructs were generated using standard PCR-based subcloning methods. Homo sapiens centrosomal protein 162 (CEP162), transcript variant 1, mRNA (Accession: NM_014895.3) was obtained from GeneCoepia (HOC20483; Rockville, MD). FLAG-tag added by overlap extension PCR to N-terminus. All DNA constructs were cloned between a 5' AgeI and a 3' NotI site, using standard T4 DNA ligation methods, and sequence confirmed. For mouse in vivo electroporation, the pRho plasmid was used (Addgene, plasmid # 11156; Watertown, MA). For mammalian cell culture, the pEGFP-N1 vector was used (Clontech, PT3027-5; Mountain View, CA). Mutagenesis was done using the QuikChange II XL kit (Stratagene, La Jolla, CA). Rho-mCherry was previously used[181].

Plasmid expression in cell culture. AD293T or IMCD3 cells were transfected at 90-95% confluency with DNA constructs mentioned above, using Lipofectamine 3000 transfection reagent (Invitrogen, L3000001). The next day, cells were incubated in complete media or serum-free media for another 24 hours before analysis.

Immunofluorescence. Supplemental Table 3 contains a complete list of antibodies and dilutions. Cetn2-GFP mouse retinal cross-sections: Immunostaining was carried out as described[101]. Briefly, fresh eyecups were embedded in OCT compound and quick-frozen in methylbutane cooled with liquid nitrogen. 10 µm thick retinal cryo-sections were blocked in 5% donkey serum and 0.05% Triton X-100 in PBS for 15 minutes before primary antibodies diluted in block for 1 hour. Sections were rinsed, fixed for 5 minutes in 1% paraformaldehyde in PBS, rinsed and incubated with secondary antibodies in block for 2 hours at 22ºC.

Electroporated mouse retinal cross-sections. The immunostaining protocol was adapted from[100]. Electroporated retinas with mCherry expression were dissected in Supplemented Mouse Ringers, pH 7.4 and ~313-320 mOsM. Fresh retinas were blocked in 10% normal donkey serum, 0.3% saponin, 1× cOmplete™ Protease (Millipore Sigma; Burlington, MA) diluted in Supplemented Mouse Ringers for 2 hours at 4°C. Primary antibodies diluted in block were incubated for 20-22 hours, rinsed and secondary antibodies incubated for 2 hours, all at 4°C. Retinas were rinsed, fixed in 4% paraformaldehyde for 30 minutes at 22°C, embedded in 4% agarose (Thermo Fisher Scientific, BP160-500), and 100 µm vibratome retinal-sections collected.

Cultured cells. 50-60×10^3 fibroblasts were plated onto 13 mm poly-L-lysine glass coverslips (Corning, 354085; Glendale, AZ) and grown overnight at 37ºC with 5% CO_2. Serum-free DMEM for 24, 48 or 72 hours to induce ciliation. Cells were placed on ice for 10 minutes before fixation in 1% paraformaldehyde for 5 minutes followed by 15 minutes in ice-cold methanol. Cells were then rinsed, permeabilized for 5 minutes with 0.1% SDS in PBS, rinsed, and blocked with 0.1% Triton-X, 5% normal donkey serum and 5% BSA

in PBS. Primary antibodies diluted in block were incubated overnight at 4ºC, rinsed, and incubated with secondary antibodies for 1 hour at 22ºC.

For all conditions, 10 µg/ml Hoechst 33342 was added with donkey secondary antibodies conjugated to Alexa Fluor 488, 568, or 647 (Jackson ImmunoResearch; West Grove, PA). Coverslips (#1.5, Electron Microscopy Sciences; Hatfield, PA) were mounted with Prolong Glass (Thermo Fisher Scientific). Images acquired using a Zeiss Observer 7 inverted microscope with a 63× oil-immersion objective (1.40 NA), LSM 800 confocal with Airyscan detector controlled by Zen 5.0 (Carl Zeiss Microscopy; White Plains, NY). Image manipulation was limited to adjusting the brightness level, image size, rotation and cropping using FIJI (ImageJ, https://imagej.net/Fiji).

Immunoprecipitation. A 10 cm plate of AD293T cells was transfected using Polyethyleneimine (PEI, Sigma 408727) at 6:1 ratio PEI:DNA with 10 µg of mock, FLAG-CEP162, or FLAG-CEP162-E646R*5 construct. After 24 hours, cells were lysed in 1% NP40 in PBS, cleared by centrifugation at 15,000 rpm for 20 min at 10°C and supernatant incubated on anti-FLAG M2 magnetic beads (Millipore Sigma, M8823) rotating overnight at 4°C. Immunoprecipitants were eluted with 100 mM 3X FLAG peptide (Millipore Sigma, F4799) in lysis buffer rotating for 1 hour at 4°C and processed for immunoblotting.

Microtubule pelleting assays. FLAG-CEP162 or FLAG-CEP162-E646R*5 immunoprecipitated in BRB80 (80 mM PIPES, 1 mM $MgCl_2$, 1 mM EGTA, ph 6.8, diluted from a 5X stock with 1x Protease Inhibitor) from 5 10 cm plates of AD293T cells was added to taxol-stabilize microtubules. The binding reaction was added on top of a 1 mL cushion (40% glycerol in BRB80 with 10 µM taxol, 1x Protease Inhibitor and 1 mM GTP)

and spun in fixed-angle rotor TLA120.1 at 76,900 rpm for 40 minutes at 25°C. Soluble and pellet fractions were collected, run on SDS-PAGE, and Western blotted for FLAG.

2.5.5 Statistics

All data represent at least 3 independent experiments. The data are presented as a mean +/- SD or SEM as indicated in the figure legends. A Welch's t test was performed using Prism9 (GraphPad) with corresponding P values listed in the legends.

2.5.6 Study approval

All individuals involved gave their informed consent prior to inclusion in this study. All investigations were conducted according to the Declaration of Helsinki, and the study was approved by the Ethics Committee of the University Hospital of Cologne, Ghent (EC UZG 2017/1540) and Brussels (A420701EI13L).

Chapter 3 Investigating The Role Of CEP162 In Promoting Terminal Cell Divisions Of RPCs During Mouse Retinal Development

3.1 Abstract

Genes encoding ciliary proteins function in both the context of the cilium and outside of it. QN1, an ortholog of CEP162, has been previously identified in terminally dividing quail retinal cell clones where it was highly expressed in cells exiting cell cycle and becoming post-mitotic neurons. It localizes to the mitotic spindles in cell culture and knockdown of QN1 causes defects in cell cycle arrest during chick retinal development. CEP162 is a microtubule associated centriolar protein required for proper transition zone assembly during ciliogenesis and in the developing mouse retina, knockdown of CEP162 increased photoreceptor cell death indicating its importance in photoreceptor cell survival during development. To study the function of CEP162 during mouse retinal development, I first established the timing of terminal cell cycle exit that gives rise to mature neurons. Immunostaining of the whole retina from P0 to P3 using PH3 to label RPCs showed gradual decrease in the number of RPCs overtime, with the sharpest decrease occurring at P3. I therefore considered P3 to be the peak of terminal cell divisions. Next, knockdown of CEP162 at P0 was achieved by *ex vivo* electroporation and retinal explant culture technique. After 3 days of culture, preliminary immunohistochemical analysis of the retinal explants revealed variable increase in the number of PH3-positive RPCs. While my data indicates CEP162 is important for cell cycle arrest of RPCs, optimization of current

experiments and further analysis is pending to determine how loss of CEP162 impacts terminal cell divisions in the developing mouse retina.

3.2 Introduction

Neurogenesis in the retina occurs through precise regulation of proliferation, terminal cell cycle exit, and differentiation of RPCs[91,94]. These multipotent progenitor cells cycle through various stages of competency in order to generate the diversity of neural cell types in the retina. In mice, ganglion cells are the first to be generated with cones, amacrine cells, and horizontal cells, all occurring embryonically. Rods are the most abundant retinal neuron and are produced throughout development with the peak occurring at birth (P0). Bipolar cells and Müller cells are generated postnatally. Importantly, there is considerable overlap when generating any of these neurons, so that at any given time cells with distinct fates are being simultaneously generated. This suggests that although RPCs are multipotent, they are not a homogeneous population, which has been confirmed by scRNA-sequencing results[182]. However, for a given RPC the transition between competence states is unidirectional so that once a specific time frame for generating a neuron has elapsed, it can no longer be generated[91,93].

An additional layer of complexity is that cycling RPCs can undergo three modes of division. In early mouse retinal development, RPCs divide producing two daughter cells with equal proliferative capacity, which is known as symmetric proliferative mode and helps increase the pool of RPCs[94]. Once the progenitor pool is expanded, RPCs switch to asymmetric differentiative mode, where one progenitor cell and one post-mitotic neuron are produced (**Figure 3-1**). Here, the distinct differentiated retinal neurons can be made while the self-renewing RPC helps maintain the progenitor pool. Early born neurons such

as cones, ganglion cells, and horizontal cells are generated from asymmetric differentiative mode. Later in mouse retinal development, the RPC pool is depleted as they switch to terminal divisions to generate two post-mitotic neurons, either with identical cell fates (symmetric) or distinct cell fates (asymmetric)[94,183,184] (**Figure 3-1**).

CEP162 is a microtubule-associated centriolar protein required for cilia formation and linked to terminal cell cycle withdrawal during retinal development. While my data supports the previous findings that CEP162 is linked to terminal cell divisions during retinal development[146,148], the molecular mechanism behind this process remains unclear. In this chapter, I explored the role of CEP162 during retinal development, specifically focusing on the hypothesis that it may regulate terminal cell cycle exit of RPC.

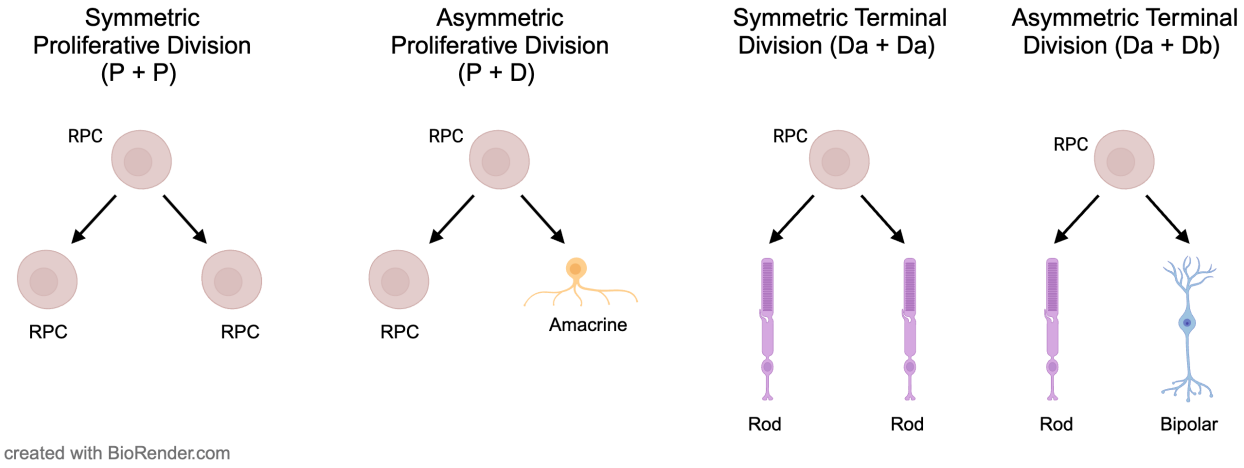

Figure 3-1 Schematic illustrating various modes of cell division that take place during retinal development.

Diagram adapted from Petridou and Godinho, 2022[94]

3.3 Determining the timing of terminal cell divisions of RPCs during mouse retinal development.

Retinogenesis culminates in terminal cell division when RPCs differentiate into post-mitotic neurons. The incorporation of nucleotide tracers such as Bromodeoxyuridine (BrdU) within the newly synthesized DNA during S-phase is commonly used to measure the rate of proliferation. If RPCs do not terminally divide and continue to proliferate, an increase in the number of BrdU-positive cells should be detected. In previous literature, knockdown of CEP162 in developing chick retinal explant cultures showed an increase in BrdU-positive cells, suggesting it may play a role in promoting RPCs entering into a terminal division mode[146]. Considering this, I hypothesized that knockdown of CEP162 during mouse retinal development will increase the number of proliferating RPCs. To investigate this possibility, I first sought to establish the number of proliferating RPCs in the mouse retina during postnatal neurogenesis, P0-P3. As a readout of progenitor cells actively proliferating, I used an antibody against phosphorylated Histone H3 (PH3), which detects histone modifications specific to the M-phase of the cell cycle[185]. PH3 labeling of the neuroretina during different stages of retinal development revealed robust rates of proliferation across the retina (**Figure 3-2**). At each timepoint, the number of RPCs proliferating per 100 μm^2 of the retina was calculated by dividing the total number of PH3-positive cells within the area of the tissue, which was selected based on DAPI staining. I found that RPC proliferation during postnatal development was maintained at a constant level until P3 when it began to gradually decrease suggesting that retinal neurogenesis in the mouse was ending (**Figure 3-2**). Interestingly, I also observed that the number of PH3-positive cells decreased more rapidly in the central retinal than in the periphery. My

analysis and observations are consistent with previous findings showing that RPCs stop dividing at P6 in the central retina and at P11 in the periphery[90].

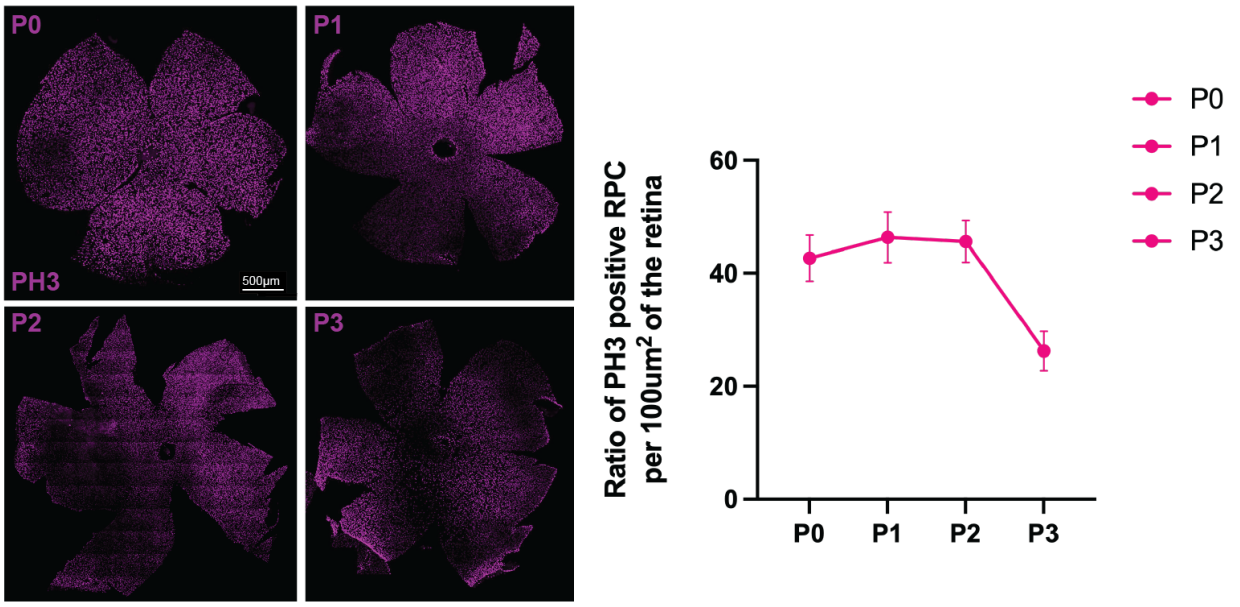

Figure 3-2 Proliferation of RPCs gradually decrease by P3 in the mouse retina.

Retinal flat mounts showing PH3-labeled RPC localization at the apical surface in the developing retina. Quantification of the ratio of PH3-labeled RPC in the retina from P0-P3.

3.4 Investigating the rate of RPC proliferation in the absence of CEP162 in the retina

To determine the role of CEP162 in terminal cell divisions, I examined how the loss of CEP162 affects the mitotic rate of RPCs during mouse retinal development. This was achieved by electroporating my shRNA constructs, which are single plasmids co-expressing either scrambled-control or CEP162-shRNA and soluble mCherry into retinal explants at P0[186]. For these experiments, I swapped the CMV promoter driving mCherry, used in cell culture (**Figure 2-5J**) for a CAG promoter after I found that the CMV promoter was not expressed in retinal neurons (data not shown). Following electroporation, retinal explants were cultured for three days, fixed, and stained with DAPI, WGA, and anti-PH3 antibodies. The apical surface of the cultured retinas was determined by WGA staining

and images were taken as ~ 30μm thick z stacks starting at the apical surface. In our preliminary analysis, PH3-positive cells were counted within the mCherry-positive areas of the retina. Quantification of PH3-positive RPCs was then normalized to the transfected area using mCherry to determine changes in the RPC proliferation in response to CEP1612 knockdown. In the absence of CEP162, I observed a subtle increase in the number of PH3-positive RPCs compared to the explant cultures electroporated with scramble shRNA control (**Figure 3-3**). Although, this data requires additional biological replicates to determine whether the result is significant, the preliminary results suggests that CEP162 is important for promoting cell cycle exit of proliferating cells.

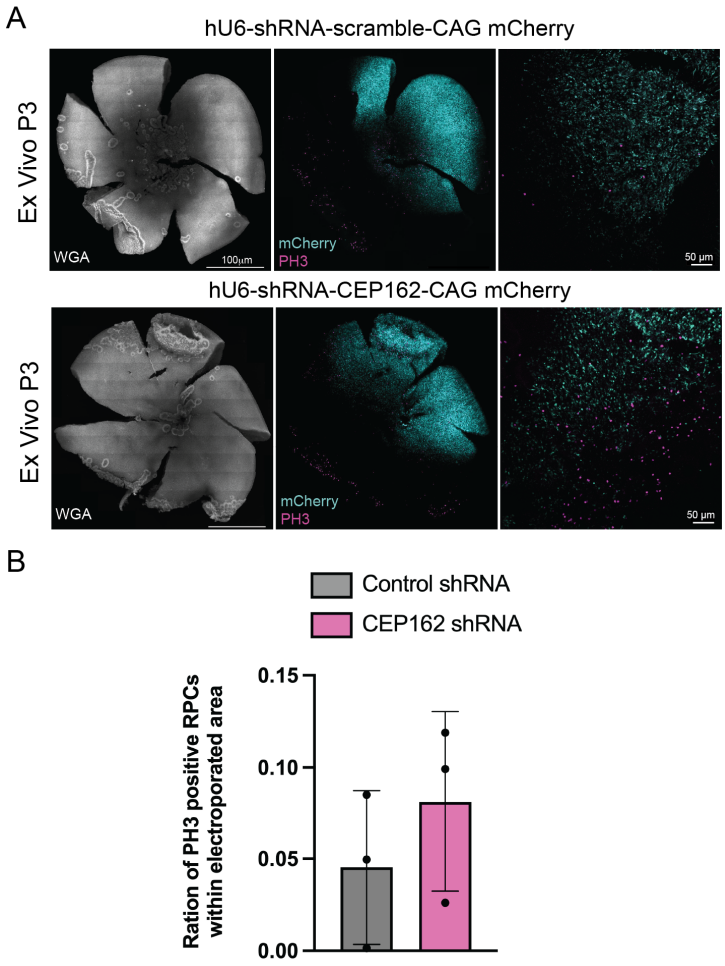

Figure 3-3 Ex vivo knockdown of CEP162 using shRNA results in an Increase in PH3-labeled RPCs compared to the control in the developing retina.

A. Flat mounts of ex vivo electroporated retinal explants collected at P3. WGA marks the apical surface, mCherry labels transfected cells, PH3 labels proliferating RPCs. B. Quantification of the ratio of PH3-labeled RPC within mCherry expressing area.

3.5 Materials and Methods.

3.5.1 Mouse studies

Albino CD-1 WT mice were from Charles River (Strain 022). All mice were housed under a 12-hour light/12-hour dark cycle. For PH3-analysis in developing mouse retina, eyes were collected from pups ranging from P0 to P3, enucleated, and fixed in 4% PFA for 2 hours. Fixed eyes were stained using immunofluorescence method described below.

3.5.2 Ex vivo electroporation

For *ex vivo* electroporation, retinal transfection of CD-1 neonatal mice was conducted as previously described (17, 37, 38). The *ex vivo* retina culture protocol was adapted from[186]. At P0, eyes were placed in neural explant media at 37°C and dissected by first creating a small puncture wound at the cornea and sclera boundary using needle (30G). Using forceps, the cornea and sclera were peeled away leaving the retina with the lens still attached. The isolated retinas were then placed in the electroporation chamber with the lens facing the metal plate. 70 µl of DNA solution was made with 25 µg/µl of shRNA plasmid DNA in 1x PBS. After electroporation, isolated retinas were placed on top of polycarbonate membrane floating in 2 ml of explant media per well in 6-well plate. 100 µl of explant media was pipetted onto the retina to encapsulate it within the growth medium. A single retina was placed on top of the membrane and cultured in each well. Explant media enclosing the retinas were changed every 24 hours. At cultured day 3, retinas were collected and fixed in 4% PFA for 2 hours before processing for immunofluorescence studies.

3.5.3 Immunofluorescence

Fixed retinas were blocked with 0.1% Triton-X, 5% normal donkey serum, and 5% BSA in PBS for 1 hour. Primary anti-PH3 antibody diluted 1:1000 in blocking buffer was incubated overnight at 4°C. The next day retinas were rinsed in PBS and then incubated with 5 µg/ml DAPI and donkey anti-mouse secondary antibodies conjugated to Alexa Fluor 488 (*Jackson ImmunoResearch*) for 1 hour at 22°C. For *ex vivo* electroporated cultured retinas, WGA conjugated to Alexa Fluor 647 was added with DAPI and secondary antibodies. Stained retina was then dissected to remove the lens and to flatten before being placed on microscope slides with apical side of the retinas facing the coverslips (no. 1.5, Electron Microscopy Sciences) and mounted using Prolong Glass (*Thermo Fisher Scientific*). The apical surface of the cultured retinas was determined by WGA staining and images were taken as ~ 30µm thick z stacks starting from the apical surface. Images were acquired using a Zeiss Observer 7 inverted microscope with a 20x objective and a LSM 800 confocal controlled by *Zen 5.0* (*Carl Zeiss Microscopy*). Image manipulation was limited to adjusting the brightness level, image size, rotation, and cropping using *FIJI (ImageJ)*.

3.5.4 Image Analysis

PH3-positive cells in the developing retina were quantified using FIJI. The polygon tool was used to measure the area of the retinas by outlining the region of interest for the nuclear counts denoted by DAPI expression. The TrackMate plugin was then used to count PH3-positive nuclei within the selected area. For *ex vivo* electroporated cultured retinas, the polygon tool was used to demarcate the electroporated area of the retina expressing shRNA and soluble mCherry. Custom analysis code written in Python was used to quantify the number of PH3-positive nuclei within the electroporated patch. This

code uses Otsu thresholding, manually adjusted as necessary, to create binarized images. These images were cleaned using erode-dilate cycles and by removing objects below a certain size threshold. The Watershed algorithm was used to segment nuclei in these cleaned binarized images, and the regionprops command was used to obtain the positions of the nuclei in the whole retina. Nuclei outside of the electroporated patch were then removed based on their positions.

Chapter 4 Conclusion And Future Direction

4.1 Conclusions

Mutations in ciliary genes cause a range of human disorders, termed ciliopathies. The light-sensitive outer segment compartment of photoreceptors is a specialized primary cilium, therefore retinal degeneration often accompanies these diseases. The function of ciliary proteins in the outer segment and how mutations in ciliary genes cause non-syndromic retinal ciliopathy continue to be an active area of study. The goal of my thesis was to determine how a novel human mutation in CEP162 resulted in non-syndromic retinal degeneration by investigating its impact on ciliogenesis and retinal neurogenesis.

CEP162 is a microtubule-associated centriolar protein required for cilium formation and linked to terminal cell cycle withdrawal during retinal development. It contains three CC domains, of which CC1 and CC2 are necessary for microtubule binding, and CC3 is required for localization to the centrioles/basal body[149]. The homozygous recessive patient mutation encodes a heavily truncated variant of CEP162 (CEP162-E646R*5) which is missing nearly all the CC domains (Figure 3-1A). Although CEP162-E646R*5 is expressed, it does not localize to the centrioles in either primary or photoreceptor cilia. I went on to show that the truncated CEP162 does not function at the cilium by showing that the reduced ciliation observed in CEP162 shRNA knockdown experiments could be rescued by full length CEP162, but not CEP162-E646R*5. Using *in-vitro* and *in-vivo* disease modeling, I uncovered dual roles for CEP162. While ciliogenesis proceeds normally in control fibroblasts, cilia assembly in the patient fibroblasts is delayed at the

stage of axoneme extension due to the persistence of CP110 at the basal body. Once ciliogenesis resumes, abnormally long cilia are built with reduced recruitment of transition zone proteins such as TMEM67 and NPHP1 (Figure 3-1B). Considering that the initial steps of outer segment development closely resemble ciliogenesis in the primary cilia, it is likely that delay in ciliogenesis and subsequent defects in the recruitment of transition zone proteins results in the late-onset retinal degeneration observed in the patient (Figure 3-1C).

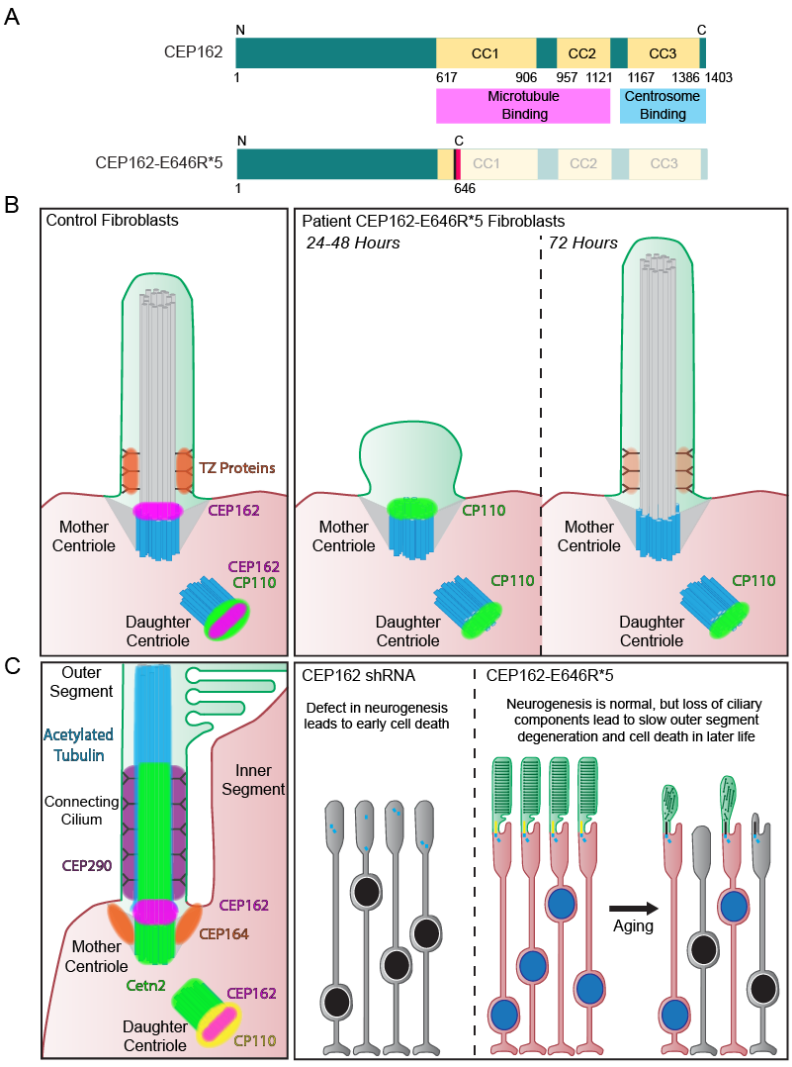

Figure 4-1 Graphical abstract summarizing the conclusions.

A. *Illustration highlighting the c-terminal CC domains of CEP162 and location of the E646R*5 mutation in CEP162.* ***B.*** *Ciliogenesis in the presence and absence of CEP162 in control and patient-derived primary fibroblasts.* ***C.*** *CEP162 localization relative to other proteins in the photoreceptor connecting cilium. CEP162 is important for neurogenesis and CEP162-E646R*5 maintains that role, while its loss of ciliary function likely results in slow outer segment degeneration.*

4.2 Future Directions and Alternative Hypothesis

4.2.1 Analyzing the changes in mitotic rates using flow cytometry in the developing retina

One of the limitations of using immunohistochemical analysis to examine mitotic rates was that I was unable to determine whether individual PH3-positive cells also expressed mCherry, which reduced our ability to precisely quantify changes caused by CEP162 knockdown. In the future, I propose to dissociate retinal explant cultures expressing my shRNA constructs (scrambled-control or CEP162-shRNA) and use flow cytometry to analyze the mitotic index. Briefly, nuclei will be fluorescently labeled with DAPI, which will allow for the dissociated cells to be sorted into distinct cell-cycle stages based on their DNA content. At G1, a single cell has 2N DNA content, while in S phase the cell is replicating the DNA content to +2N-4N. In G2/M phase, a single cell has 4N DNA content before cytokinesis splits it between two separate daughter cells. As DAPI gets incorporated during these stages in proportion to the DNA content of each cell, it can be used to sort cells into the different phases of cell cycle. Multiparametric analysis using other cell-cycle markers such as EdU, Ki-67, or PH3 could be done to distinguish individual cell population[187–189]. P0 retinal explants will be electroporated with shRNA constructs (scrambled-control or CEP162-shRNA) that also express soluble mCherry. At P3, these retinas will be collected and dissociated prior to running flow cytometry. Transfected cells will be sorted using mCherry-expression and then sorted according to their DNA content (DAPI). The cells will be further sorted based on their DNA content and EdU incorporation to distinguish cells in S-Phase. If more RPCs remain proliferative in response to CEP162 knockdown, I expect to see an increase in the number of cells in the

S and G2/M phases of the flow cytometry plot in the CEP162-shRNA expressing cells compared to the scrambled shRNA control. Additionally, if failure to terminally divide results in cell death, labeling the dissociated cells with impermeant nucleic acid dyes along with DAPI, will help sort dead cells with compromised membrane barrier from live cells with intact membrane barrier.

Finally, to determine whether CEP162 is required for terminal cell cycle entry of RPCs, rescue experiments co-expressing FLAG-tagged CEP162 will be performed in the retinal explants with siRNA against CEP162 or control siRNA. I expect to see rescue of the increase in proliferation observed in the absence of CEP162. Since I hypothesize that CEP162 localization at the mitotic spindle through direct microtubule-binding is required for its neurogenesis function, I propose to co-express a CEP162 mutant construct that truncates all the CC domains (CEP162-ΔCC), previously shown to be important for microtubule binding[149]. Here, I expect that while co-expressing full-length CEP162 with the CEP162 shRNA would rescue the proliferation defect, co-expression of CEP162-ΔCC would fail to reduce the elevated number of RPCs observed in imaging experiments and by flow cytometry.

4.2.2 Localization of CEP162 at the mitotic spindle could promote proper spindle orientation which is required for terminal cell divisions in the retina

During retinal development, RPC nuclei move bidirectionally from the apical-basal surface relative to phases of their cell cycle, through a process known as interkinetic nuclear migration (INM)[190,191]. As cells cycle, S phase occurs near basal side of the neuroblast while mitosis is restricted to the apical surface. This highly conserved process relies on precise control of nuclear positioning and spindle pole orientation[184,192–194] as RPCs orient

their mitotic spindles to match growth factor distribution. Ligand-induced signaling pathway, such as notch, is distributed in a gradient with high notch activity at the apical surface and low notch activity at the basal neuroepithelium[195]. Alignment of the mitotic spindles parallel to the plane of the neuroepithelium produces identical proliferative progenitor cells, where notch signaling is high. Alternatively, perpendicular positioning of the mitotic spindles to the neuroepithelium gives rise to one self-renewing RPC in high notch zone and one differentiating neuron exposed to lower notch concentration. Further nuclear movement of progenitors to the basal surface produces two post-mitotic neurons in response to low notch activity at that region[195,196].

My data demonstrated that both full-length CEP162 and patient CEP162-E646R*5 localized to the mitotic spindle, and directly bind to microtubules *in vitro*. In the future, it will be interesting to observe whether the loss of CEP162 affects spindle orientation. To start, retinas from Cetn2-GFP transgenic mice could be used to observe the normal distribution of spindle orientation in RPCs during retinal development. Centrin 2 localizes to both centrioles and in Cetn2-GFP mice, centrioles in every organ and tissue are constitutively expressing cetn2-GFP at every time point[158]. Retinas could be collected at P3 and then fixed, sectioned, and stained with PH3, DAPI, α-tubulin. Quantification of spindle orientation relative to the neuroblast plane would establish the normal physiological distribution of parallel and perpendicular planes of spindle orientation in RPCs.

To assess how the loss of CEP162 affects spindle orientation, Cetn2-GFP mouse eyes would be electroporated at P0 with either control shRNA or shRNA against CEP162 and soluble mCherry to visualize transfected cells. At P3, retinas would be collected,

fixed, sectioned, and stained with PH3, DAPI, and α-tubulin. If CEP162 is necessary for proper alignment of the mitotic spindle during terminal cell division, then in the absence of CEP162, defects in this alignment will prevent INM of mCherry labeled RPCs towards the lower notch zone at the basal surface and thus these RPCs will remain proliferative at the apical surface. Quantification of the spindle orientation of these RPCs will also reveal an increase in the parallel alignment of the spindles compared to the RPCs in the control retinas.

Together, these potential future projects would expand our understanding of the role of CEP162 during neurogenesis. It would also provide us with valuable mechanistic insights into how centriolar proteins function during the cell cycle and how they are utilized to balance proliferation and differentiation of RPCs into neurons in the retina.

Bibliography

1. Carvalho-Santos, Z., Azimzadeh, J., Pereira-Leal, José. B. & Bettencourt-Dias, M. Tracing the origins of centrioles, cilia, and flagella. *Journal of Cell Biology* **194**, 165–175 (2011).
2. Margulis, L., Chapman, M., Guerrero, R. & Hall, J. *The last eukaryotic common ancestor (LECA): Acquisition of cytoskeletal motility from aerotolerant spirochetes in the Proterozoic Eon*. www.pnas.orgcgidoi10.1073pnas.0604985103 (2006).
3. Bloodgood, R. A. From central to rudimentary to primary: the history of an underappreciated organelle whose time has come. The primary cilium. *Methods in cell biology* vol. 94 2–52 Preprint at https://doi.org/10.1016/s0091-679x(08)94001-2 (2009).
4. Goetz, S. C. & Anderson, K. V. The primary cilium: A signalling centre during vertebrate development. *Nature Reviews Genetics* vol. 11 331–344 Preprint at https://doi.org/10.1038/nrg2774 (2010).
5. Corbit, K. C. *et al.* Vertebrate Smoothened functions at the primary cilium. *Nature* **437**, 1018–1021 (2005).
6. Gulati, S. & Palczewski, K. Structural view of G protein-coupled receptor signaling in the retinal rod outer segment. *Trends in Biochemical Sciences* vol. 48 172–186 Preprint at https://doi.org/10.1016/j.tibs.2022.08.010 (2023).

7. Pearring, J. N., Salinas, R. Y., Baker, S. A. & Arshavsky, V. Y. Protein sorting, targeting and trafficking in photoreceptor cells. *Progress in Retinal and Eye Research* vol. 36 24–51 Preprint at https://doi.org/10.1016/j.preteyeres.2013.03.002 (2013).

8. Scholey, J. The sensory cilia of Caenorhabditis elegans_Revised. *WormBook* (2007) doi:10.1895/wormbook.1.126.2.

9. O'Toole, E. T., Giddings, T. H., McIntosh, J. R. & Dutcher, S. K. Three-dimensional organization of basal bodies from wild-type and δ-tubulin deletion strains of Chlamydomonas reinhardtii. *Mol Biol Cell* **14**, 2999–3012 (2003).

10. Satir, P. & Christensen, S. T. Overview of structure and function of mammalian cilia. *Annual Review of Physiology* vol. 69 377–400 Preprint at https://doi.org/10.1146/annurev.physiol.69.040705.141236 (2007).

11. Kiesel, P. *et al.* The molecular structure of mammalian primary cilia revealed by cryo-electron tomography. *Nat Struct Mol Biol* **27**, 1115–1124 (2020).

12. Klena, N. & Pigino, G. Structural Biology of Cilia and Intraflagellar Transport. (2022) doi:10.1146/annurev-cellbio-120219.

13. Li, S., Fernandez, J. J., Fabritius, A. S., Agard, D. A. & Winey, M. Electron cryo-tomography structure of axonemal doublet microtubule from Tetrahymena thermophila. *Life Sci Alliance* **5**, (2022).

14. Ishikawa, T. Cryo-electron tomography of motile cilia and flagella. *Cilia* Preprint at https://doi.org/10.1186/s13630-014-0012-7 (2015).

15. Ishikawa, T. 3D structure of eukaryotic flagella/cilia by cryo-electron tomography. *Biophysics (Japan)* vol. 9 141–148 Preprint at https://doi.org/10.2142/biophysics.9.141 (2013).

16. Jana, S. C. Centrosome structure and biogenesis: Variations on a theme? *Seminars in Cell and Developmental Biology* vol. 110 123–138 Preprint at https://doi.org/10.1016/j.semcdb.2020.10.014 (2021).
17. Lee, L. & Ostrowski, L. E. Motile cilia genetics and cell biology: big results from little mice. *Cellular and Molecular Life Sciences* vol. 78 769–797 Preprint at https://doi.org/10.1007/s00018-020-03633-5 (2021).
18. Burgess, S. A., Walker, M. L., Sakakibara, H., Knight, P. J. & Oiwa, K. Dynein structure and power stroke. *Nature* **421**, (2003).
19. Legendre, M., Zaragosi, L. E. & Mitchison, H. M. Motile cilia and airway disease. *Seminars in Cell and Developmental Biology* vol. 110 19–33 Preprint at https://doi.org/10.1016/j.semcdb.2020.11.007 (2021).
20. Yuan, S. *et al.* Oviductal motile cilia are essential for oocyte pickup but dispensable for sperm and embryo transport. *PNAS* **118**, (2021).
21. Ringers, C., Olstad, E. W. & Jurisch-Yaksi, N. The role of motile cilia in the development and physiology of the nervous system. *Philosophical Transactions of the Royal Society B: Biological Sciences* vol. 375 Preprint at https://doi.org/10.1098/rstb.2019.0156 (2020).
22. Hirokawa, N., Tanaka, Y. & Okada, Y. Cilia, KIF3 molecular motor and nodal flow. *Current Opinion in Cell Biology* vol. 24 31–39 Preprint at https://doi.org/10.1016/j.ceb.2012.01.002 (2012).
23. Lehti, M. S. & Sironen, A. Formation and function of sperm tail structures in association with sperm motility defects. *Biology of Reproduction* vol. 97 522–536 Preprint at https://doi.org/10.1093/biolre/iox096 (2017).

24. Yoshimura, K. A novel type of mechanoreception by the flagella of Chlamydomonas_yoshimura_1996. *Journal of Experimental Biology* **199**, 295–302 (1996).

25. Fujiu, K., Nakayama, Y., Iida, H., Sokabe, M. & Yoshimura, K. Mechanoreception in motile flagella of Chlamydomonas. *Nat Cell Biol* **13**, 630–632 (2011).

26. Barnes, C. L., Malhotra, H. & Calvert, P. D. Compartmentalization of Photoreceptor Sensory Cilia. *Frontiers in Cell and Developmental Biology* vol. 9 Preprint at https://doi.org/10.3389/fcell.2021.636737 (2021).

27. Flock, A. & Duvall, A. J. The ultrastructure of the kinocilium of the sensory cells in the inner ear and lateral line organs. *Journal of Cell Biology* **25**, (1965).

28. Jenkins, P. M., Mcewen, D. P. & Martens, J. R. Olfactory cilia: Linking sensory cilia function and human disease. *Chem Senses* **34**, 451–464 (2009).

29. Pazour, G. J. *et al. Chlamydomonas IFT 88 and Its Mouse Homologue, Polycystic Kidney Disease Gene Tg 737, Are Required for Assembly of Cilia and Flagella*. *The Journal of Cell Biology* vol. 151 http://www.jcb.org/cgi/content/full/151/3/709 (2000).

30. Sorokin, S. P. Reconstructions of centriole formation and ciliogenesis in mammalian lungs. *J. Cell Sci* **3**, 207–230 (1968).

31. Sorokin, S. CENTRIOLES AND THE FORMATION OF RUDIMENTARY CILIA BY FIBROBLASTS AND SMOOTH MUSCLE CELLS. *J Cell Biol* **15**, 363–377 (1962).

32. Graser, S. *et al.* Cep164, a novel centriole appendage protein required for primary cilium formation. *Journal of Cell Biology* **179**, 321–330 (2007).

33. Sillibourne, J. E. *et al.* Assessing the localization of centrosomal proteins by PALM/STORM nanoscopy. *Cytoskeleton* **68**, 619–627 (2011).

34. Joo, K. *et al.* CCDC41 is required for ciliary vesicle docking to the mother centriole. *Proc Natl Acad Sci U S A* **110**, 5987–5992 (2013).

35. Tanos, B. E. *et al.* Centriole distal appendages promote membrane docking, leading to cilia initiation. *Genes Dev* **27**, 163–168 (2013).

36. Yang, T. T. *et al.* Super-resolution architecture of mammalian centriole distal appendages reveals distinct blade and matrix functional components. *Nat Commun* **9**, (2018).

37. Chong, W. M. *et al.* Super-resolution microscopy reveals coupling between mammalian centriole subdistal appendages and distal appendages. *Elife* **9**, (2020).

38. Knödler, A. *et al.* Coordination of Rab8 and Rab11 in primary ciliogenesis. *Proc Natl Acad Sci U S A* **107**, 6346–6351 (2010).

39. Moritz, O. L. *et al. Mutant rab8 Impairs Docking and Fusion of Rhodopsin-bearing Post-Golgi Membranes and Causes Cell Death of Transgenic Xenopus Rods*. *Molecular Biology of the Cell* vol. 12 (2001).

40. Westlake, C. J. *et al.* Primary cilia membrane assembly is initiated by Rab11 and transport protein particle II (TRAPPII) complex-dependent trafficking of Rabin8 to the centrosome. *Proc Natl Acad Sci U S A* **108**, 2759–2764 (2011).

41. Wu, C. T., Chen, H. Y. & Tang, T. K. Myosin-Va is required for preciliary vesicle transportation to the mother centriole during ciliogenesis. *Nat Cell Biol* **20**, 175–185 (2018).

42. Schmidt, K. N. *et al.* Cep164 mediates vesicular docking to the mother centriole during early steps of ciliogenesis. *Journal of Cell Biology* **199**, 1083–1101 (2012).

43. Lu, Q. *et al.* Early steps in primary cilium assembly require EHD1/EHD3-dependent ciliary vesicle formation. *Nat Cell Biol* **17**, 228–240 (2015).

44. Ganga, A. K. *et al.* Rab34 GTPase mediates ciliary membrane formation in the intracellular ciliogenesis pathway. *Current Biology* **31**, 2895-2905.e7 (2021).

45. Stuck, M. W., Chong, W. M., Liao, J. C. & Pazour, G. J. Rab34 is necessary for early stages of intracellular ciliogenesis. *Current Biology* **31**, 2887-2894.e4 (2021).

46. Insinna, C. *et al.* Investigation of F-BAR domain PACSIN proteins uncovers membrane tubulation function in cilia assembly and transport. *Nat Commun* **10**, (2019).

47. Johnson, K. A. & Rosenbaum, J. L. Replication of basal bodies and centrioles. *Curr Opin Cell Biol* **4**, 80–85 (1992).

48. Hao, L. *et al.* Intraflagellar transport delivers tubulin isotypes to sensory cilium middle and distal segments. *Nat Cell Biol* **13**, 790–798 (2011).

49. Kozminski, K. G., Beech, P. L. & Rosenbaum, J. L. The Chlamydomonas kinesin-like protein FLA10 is involved in motility associated with the flagellar membrane. *J Cell Biol* **131**, 1517–1527 (1995).

50. Taschner, M., Bhogaraju, S. & Lorentzen, E. Architecture and function of IFT complex proteins in ciliogenesis. *Differentiation* **83**, (2012).

51. Adams, G. M. W., Huang, B. & Luck, D. J. L. Temperature sensitive assembly and assembly defective flagella mutants of chlamydomonas reinhardtii. *Genetics* **100**, 579–586 (1982).

52. Inglis, P. N., Ou, G., Leroux, M. R. & Scholey, J. M. The sensory cilia of Caenorhabditis elegans. *WormBook* 1–22 (2007) doi:10.1895/wormbook.1.126.2.

53. Garcia-Gonzalo, F. R. & Reiter, J. F. Open Sesame: How transition fibers and the transition zone control ciliary composition. *Cold Spring Harb Perspect Biol* **9**, (2017).

54. Chih, B. *et al.* A ciliopathy complex at the transition zone protects the cilia as a privileged membrane domain. *Nat Cell Biol* **14**, 61–72 (2012).

55. Dowdle, W. E. *et al.* Disruption of a ciliary B9 protein complex causes meckel syndrome. *Am J Hum Genet* **89**, 94–110 (2011).

56. Mollet, G. *et al.* The gene mutated in juvenile nephronophthisis type 4 encodes a novel protein that interacts with nephrocystin. *Nat Genet* **32**, 300–305 (2002).

57. Arts, H. H. *et al.* Mutations in the gene encoding the basal body protein RPGRIP1L, a nephrocystin-4 interactor, cause Joubert syndrome. *Nat Genet* **39**, 882–888 (2007).

58. Sang, L. *et al.* Mapping the NPHP-JBTS-MKS protein network reveals ciliopathy disease genes and pathways. *Cell* **145**, 513–528 (2011).

59. Garcia-Gonzalo, F. R. & Reiter, J. F. Scoring a backstage pass: Mechanisms of ciliogenesis and ciliary access. *Journal of Cell Biology* **197**, 697–709 (2012).

60. Huang, L. *et al.* TMEM237 is mutated in individuals with a Joubert syndrome related disorder and expands the role of the TMEM family at the ciliary transition zone. *Am J Hum Genet* **89**, 713–730 (2011).

61. Christopher, K. J., Wang, B., Kong, Y. & Weatherbee, S. D. Forward genetics uncovers Transmembrane protein 107 as a novel factor required for ciliogenesis and Sonic hedgehog signaling. *Dev Biol* **368**, 382–392 (2012).

62. Barker, A. R., Renzaglia, K. S., Fry, K. & Dawe, H. R. Bioinformatic analysis of ciliary transition zone proteins reveals insights into the evolution of ciliopathy networks. *BMC Genomics* **15**, (2014).

63. Roberson, E. C. *et al.* TMEM231, mutated in orofaciodigital and Meckel syndromes, organizes the ciliary transition zone. *Journal of Cell Biology* **209**, 129–142 (2015).

64. Lambacher, N. J. *et al.* TMEM107 recruits ciliopathy proteins to subdomains of the ciliary transition zone and causes Joubert syndrome. *Nat Cell Biol* **18**, 122–131 (2016).

65. Williams, C. L. *et al.* MKS and NPHP modules cooperate to establish basal body/transition zone membrane associations and ciliary gate function during ciliogenesis. *Journal of Cell Biology* **192**, 1023–1041 (2011).

66. Jensen, V. L. *et al.* Formation of the transition zone by Mks5/Rpgrip1L establishes a ciliary zone of exclusion (CIZE) that compartmentalises ciliary signalling proteins and controls PIP 2 ciliary abundance . *EMBO J* **34**, 2537–2556 (2015).

67. Nachury, M. V. The molecular machines that traffic signaling receptors into and out of cilia. *Current Opinion in Cell Biology* vol. 51 124–131 Preprint at https://doi.org/10.1016/j.ceb.2018.03.004 (2018).

68. Nachury, M. V. & Mick, D. U. Establishing and regulating the composition of cilia for signal transduction. *Nat Rev Mol Cell Biol* **20**, 389–405 (2019).

69. Kobayashi, T., Tsang, W. Y., Li, J., Lane, W. & Dynlacht, B. D. Centriolar kinesin Kif24 interacts with CP110 to remodel microtubules and regulate ciliogenesis. *Cell* **145**, 914–925 (2011).

70. Schmidt, T. I. *et al.* Control of Centriole Length by CPAP and CP110. *Current Biology* **19**, 1005–1011 (2009).

71. Lee, M., Seo, M. Y., Chang, J., Hwang, D. S. & Rhee, K. PLK4 phosphorylation of CP110 is required for efficient centriole assembly. *Cell Cycle* **16**, 1225–1234 (2017).

72. Spektor, A., Tsang, W. Y., Khoo, D. & Dynlacht, B. D. Cep97 and CP110 Suppress a Cilia Assembly Program. *Cell* **130**, 678–690 (2007).

73. Tsang, W. Y. *et al.* CP110 Suppresses Primary Cilia Formation through Its Interaction with CEP290, a Protein Deficient in Human Ciliary Disease. *Dev Cell* **15**, 187–197 (2008).

74. Yadav, S. P. *et al.* Centrosomal protein CP110 controls maturation of the mother centriole during cilia biogenesis. *Development (Cambridge)* **143**, 1491–1501 (2016).

75. Čajánek, L. & Nigg, E. A. Cep164 triggers ciliogenesis by recruiting Tau tubulin kinase 2 to the mother centriole. *Proc Natl Acad Sci U S A* **111**, (2014).

76. Goetz, S. C., Liem, K. F. & Anderson, K. V. The spinocerebellar ataxia-associated gene tau tubulin kinase 2 controls the initiation of ciliogenesis. *Cell* **151**, 847–858 (2012).

77. Huang, N. *et al.* M-Phase Phosphoprotein 9 regulates ciliogenesis by modulating CP110-CEP97 complex localization at the mother centriole. *Nat Commun* **9**, (2018).

78. Kuhns, S. *et al.* The microtubule affinity regulating kinase MARK4 promotes axoneme extension during early ciliogenesis. *Journal of Cell Biology* **200**, 505–522 (2013).

79. Hurov, J. & Piwnica-Worms, H. The Par-1/MARK family of protein kinases: From polarity to metabolism. *Cell Cycle* vol. 6 1966–1969 Preprint at https://doi.org/10.4161/cc.6.16.4576 (2007).

80. Moroni, R. F., De Biasi, S., Colapietro, P., Larizza, L. & Beghini, A. Distinct expression pattern of microtubule-associated protein/microtubule affinity-regulating kinase 4 in differentiated neurons. *Neuroscience* **143**, 83–94 (2006).

81. Wheway, G., Nazlamova, L. & Hancock, J. T. Signaling through the primary cilium. *Frontiers in Cell and Developmental Biology* vol. 6 Preprint at https://doi.org/10.3389/fcell.2018.00008 (2018).

82. Oh, E. C. & Katsanis, N. Context-dependent regulation of Wnt signaling through the primary cilium. *Journal of the American Society of Nephrology* vol. 24 10–18 Preprint at https://doi.org/10.1681/ASN.2012050526 (2013).

83. Malhotra, H., Barnes, C. L. & Calvert, P. D. Functional compartmentalization of photoreceptor neurons. *Pflugers Archiv European Journal of Physiology* vol. 473 1493–1516 Preprint at https://doi.org/10.1007/s00424-021-02558-7 (2021).

84. Wässle, H. Parallel processing in the mammalian retina. *Nature Reviews Neuroscience* vol. 5 747–757 Preprint at https://doi.org/10.1038/nrn1497 (2004).

85. Masland, R. H. The Neuronal Organization of the Retina. *Neuron* vol. 76 266–280 Preprint at https://doi.org/10.1016/j.neuron.2012.10.002 (2012).

86. Reichenbach, A. & Bringmann, A. Glia of the human retina. *Glia* **68**, 768–796 (2020).

87. Belecky-Adams, T. *et al.* Pax-6, Prox 1, and Chx10 homeobox gene expression correlates with phenotypic fate of retinal precursor cells. *Invest Ophthalmol Vis Sci* **38**, 1293–303 (1997).

88. Rapaport, D. H., Wong, L. L., Wood, E. D., Yasumura, D. & LaVail, M. M. Timing and topography of cell genesis in the rat retina. *J Comp Neurol* **474**, 304–324 (2004).

89. Wong, L. L. & Rapaport, D. H. Defining retinal progenitor cell competence in *Xenopus laevis* by clonal analysis. *Development* **136**, 1707–1715 (2009).

90. Young, R. W. Cell differentiation in the retina of the mouse. *Anat Rec* **212**, 199–205 (1985).

91. Cepko, C. Intrinsically different retinal progenitor cells produce specific types of progeny. *Nature Reviews Neuroscience* vol. 15 615–627 Preprint at https://doi.org/10.1038/nrn3767 (2014).

92. Carter-Dawson, L. D. & Lavail, M. M. Rods and cones in the mouse retina. II. Autoradiographic analysis of cell generation using tritiated thymidine. *J Comp Neurol* **188**, 263–272 (1979).

93. Cepko, C. L. The Determination of Rod and Cone Photoreceptor Fate. *Annu Rev Vis Sci* **1**, 211–234 (2015).

94. Petridou, E. & Godinho, L. Cellular and Molecular Determinants of Retinal Cell Fate. *The Annual Review of Vision Science* **8**, 79–99 (2022).

95. Cook, T. & Desplan, C. Photoreceptor subtype specification: From flies to humans. *Semin Cell Dev Biol* **12**, 509–518 (2001).

96. Arshavsky, V. Y., Lamb, T. D. & Pugh, E. N. G proteins and phototransduction. *Annual Review of Physiology* vol. 64 153–187 Preprint at https://doi.org/10.1146/annurev.physiol.64.082701.102229 (2002).

97. Molday, R. S. & Moritz, O. L. Photoreceptors at a glance. *J Cell Sci* **128**, 4039–4045 (2015).

98. Gilliam, J. C. *et al.* Three-dimensional architecture of the rod sensory cilium and its disruption in retinal neurodegeneration. *Cell* **151**, 1029–1041 (2012).

99. Nickell, S., Park, P. S.-H., Baumeister, W. & Palczewski, K. Three-dimensional architecture of murine rod outer segments determined by cryoelectron tomography. *J Cell Biol* **177**, 917–925 (2007).

100. Robichaux, M. A. *et al.* Defining the layers of a sensory cilium with STORM and cryoelectron nanoscopy. *Proc Natl Acad Sci U S A* **116**, 23562–23572 (2019).

101. Hong, D. H., Yue, G., Adamian, M. & Li, T. Retinitis Pigmentosa GTPase Regulator (RPGR)-interacting Protein Is Stably Associated with the Photoreceptor Ciliary Axoneme and Anchors RPGR to the Connecting Cilium. *Journal of Biological Chemistry* **276**, 12091–12099 (2001).

102. Murga-Zamalloa, C. A., Swaroop, A. & Khanna, H. RPGR-containing protein complexes in syndromic and non-syndromic retinal degeneration due to ciliary dysfunction. *J Genet* **88**, 399–407 (2009).

103. Dharmat, R. *et al.* SPATA7 maintains a novel photoreceptor-specific zone in the distal connecting cilium. *Journal of Cell Biology* **217**, 2851–2865 (2018).

104. Sedmak, T. & Wolfrum, U. Intraflagellar transport proteins in ciliogenesis of photoreceptor cells. *Biol Cell* **103**, 449–466 (2011).

105. Whiteley, H. E. & Young, S. Cilia in the fetal and neonatal canine retina. *Tissue Cell* **17**, 335–340 (1985).

106. Greiner, J. V, Weidman~, T. A., Daniel Bodley$, H. & Greinerii, C. A. M. *Ciliogenesis in Photoreceptor Cells of the Retina*. *Exp. Eye Res. (t981)* vol. 33.

107. Moye, A. R., Robichaux, M. A. & Wensel, T. Expansion Microscopy of Mouse Photoreceptor Cilia. in 395–402 (2023). doi:10.1007/978-3-031-27681-1_58.

108. Reed, M., Takemaru, K.-I., Ying, G., Frederick, J. M. & Baehr, W. Deletion of CEP164 in mouse photoreceptors post-ciliogenesis interrupts ciliary intraflagellar transport (IFT) 2 3. doi:10.1101/2022.03.21.485080.

109. Gilula, N. & Satir, P. THE CILIARY NECKLACE : A Ciliary Membrane Specialization. *Journal of Cell Biology* **53**, 494–509 (1972).

110. Spencer, W. J. & Arshavsky, V. Y. A Ciliary Branched Actin Network Drives Photoreceptor Disc Morphogenesis. *Adv Exp Med Biol* **1415**, 507–511 (2023).

111. Spencer, W. J. *et al.* Photoreceptor disc membranes are formed through an Arp2/3-dependent lamellipodium-like mechanism. doi:10.1073/pnas.1913518117/-/DCSupplemental.

112. Hartong, D. T., Berson, E. L. & Dryja, T. P. Retinitis pigmentosa. *The Lancet* **368**, 1795–1809 (2006).

113. Milstein, M. L. *et al.* Multistep peripherin-2/rds self-assembly drives membrane curvature for outer segment disk architecture and photoreceptor viability. *NEUROSCIENCE Downloaded at UNIVERSITY OF MICHIGAN on February* **24**, 2020.

114. Vasquez, S. S. V., van Dam, J. & Wheway, G. An updated SYSCILIA gold standard (SCGSv2) of known ciliary genes, revealing the vast progress that has been made in the cilia research field. *Mol Biol Cell* **32**, (2021).

115. Van Dam, T. J. P. *et al.* Ciliacarta: An integrated and validated compendium of ciliary genes. *PLoS One* **14**, (2019).

116. Turan, M. G., Orhan, M. E., Cevik, S. & Kaplan, O. I. CiliaMiner: an integrated database for ciliopathy genes and ciliopathies. *Database (Oxford)* **2023**, (2023).

117. Panizzi, J. R. *et al.* CCDC103 mutations cause primary ciliary dyskinesia by disrupting assembly of ciliary dynein arms. *Nat Genet* **44**, 714–719 (2012).

118. Hjeij, R. *et al.* CCDC151 mutations cause primary ciliary dyskinesia by disruption of the outer dynein arm docking complex formation. *Am J Hum Genet* **95**, 257–274 (2014).

119. Narasimhan, V. *et al.* Mutations in CCDC11, which Encodes a Coiled-Coil Containing Ciliary Protein, Causes Situs Inversus Due to Dysmotility of Monocilia in the Left-Right Organizer. *Hum Mutat* **36**, 307–318 (2015).

120. Noone, P. G. *et al.* Primary Ciliary Dyskinesia. *Am J Respir Crit Care Med* **169**, 459–467 (2004).

121. Wallmeier, J. *et al.* Motile ciliopathies. *Nat Rev Dis Primers* **6**, (2020).

122. Failler, M. *et al.* Mutations of CEP83 cause infantile nephronophthisis and intellectual disability. *Am J Hum Genet* **94**, 905–914 (2014).

123. Chaki, M. *et al.* Exome capture reveals ZNF423 and CEP164 mutations, linking renal ciliopathies to DNA damage response signaling. *Cell* **150**, 533–548 (2012).

124. Gonçalves, A. B. *et al.* CEP78 functions downstream of CEP350 to control biogenesis of primary cilia by negatively regulating CP110 levels. *Elife* **10**, (2021).

125. Thomas, S. *et al.* A Homozygous PDE6D Mutation in Joubert Syndrome Impairs Targeting of Farnesylated INPP5E Protein to the Primary Cilium. *Hum Mutat* **35**, 137–146 (2014).

126. Leightner, A. C. *et al.* The meckel syndrome protein meckelin (TMEM67) is a key regulator of cilia function but is not required for tissue planar polarity. *Hum Mol Genet* **22**, 2024–2040 (2013).

127. Valente, E. M. *et al.* Mutations in CEP290, which encodes a centrosomal protein, cause pleiotropic forms of Joubert syndrome. *Nat Genet* **38**, 623–625 (2006).

128. Beigi, F. *et al.* Homozygous females for a X-linked RPGR-ORF15 mutation in an Iranian family with retinitis pigmentosa. *Exp Eye Res* **211**, (2021).

129. Gan, D. K., He, C. L., Shu, H. R., Hoffman, M. R. & Jin, Z. B. Novel RPGR-ORF15 mutations in X-linked retinitis pigmentosa patients. *Neurosci Lett* **500**, 16–19 (2011).

130. Dryja, T. P. *et al. Null RPGRIP1 Alleles in Patients with Leber Congenital Amaurosis*. *Am. J. Hum. Genet* vol. 68 (2001).

131. Wright, A. F., Chakarova, C. F., Abd El-Aziz, M. M. & Bhattacharya, S. S. Photoreceptor degeneration: Genetic and mechanistic dissection of a complex trait. *Nature Reviews Genetics* vol. 11 273–284 Preprint at https://doi.org/10.1038/nrg2717 (2010).

132. Hamel, C. Retinitis pigmentosa. *Orphanet J Rare Dis* **1**, 40 (2006).

133. Liu, W., Liu, S., Li, P. & Yao, K. Retinitis Pigmentosa: Progress in Molecular Pathology and Biotherapeutical Strategies. *International Journal of Molecular Sciences* vol. 23 Preprint at https://doi.org/10.3390/ijms23094883 (2022).

134. Bramall, A. N., Wright, A. F., Jacobson, S. G. & McInnes, R. R. The genomic, biochemical, and cellular responses of the retina in inherited photoreceptor degenerations and prospects for the treatment of these disorders. *Annual Review of Neuroscience* vol. 33 441–472 Preprint at https://doi.org/10.1146/annurev-neuro-060909-153227 (2010).

135. Bhardwaj, A., Yadav, A., Yadav, M. & Tanwar, M. Genetic dissection of non-syndromic retinitis pigmentosa. *Indian Journal of Ophthalmology* vol. 70 2355–2385 Preprint at https://doi.org/10.4103/ijo.IJO_46_22 (2022).

136. Brunk, K. *et al.* Cep78 is a new centriolar protein involved in Plk4-induced centriole overduplication. *J Cell Sci* **129**, 2713–2718 (2016).

137. Lähteenoja, L. *et al.* A novel frameshift variant in CEP78 associated with nonsyndromic retinitis pigmentosa, and a review of CEP78-related phenotypes. *Ophthalmic Genetics* vol. 43 152–158 Preprint at https://doi.org/10.1080/13816810.2022.2045511 (2022).

138. Chen, H. Y., Kelley, R. A., Li, T. & Swaroop, A. Primary cilia biogenesis and associated retinal ciliopathies. *Seminars in Cell and Developmental Biology* vol. 110 70–88 Preprint at https://doi.org/10.1016/j.semcdb.2020.07.013 (2021).

139. Batman, U., Deretic, J., Firat-Karalar, N. & Firat-Karalar, E. N. The ciliopathy protein CCDC66 controls mitotic progression and cytokinesis by promoting microtubule nucleation and organization. *BioRxiv* (2022) doi:10.1101/2022.04.22.489036.

140. Taulet, N. *et al.* IFT88 controls NuMA enrichment at k-fibers minus-ends to facilitate their re-anchoring into mitotic spindles. *Sci Rep* **9**, (2019).

141. Xie, Z. *et al.* Cep120 and TACCs Control Interkinetic Nuclear Migration and the Neural Progenitor Pool. *Neuron* **56**, 79–93 (2007).

142. Al-Jassar, C. *et al.* The Ciliopathy-Associated Cep104 Protein Interacts with Tubulin and Nek1 Kinase. *Structure* **25**, 146–156 (2017).

143. Karasu, O. R., Neuner, A., Atorino, E. S., Pereira, G. & Schiebel, E. The central scaffold protein CEP350 coordinates centriole length, stability, and maturation. *Journal of Cell Biology* **221**, (2022).

144. Hua, K. & Ferland, R. J. Primary cilia proteins: ciliary and extraciliary sites and functions. *Cellular and Molecular Life Sciences* vol. 75 1521–1540 Preprint at https://doi.org/10.1007/s00018-017-2740-5 (2018).

145. Bidou, L., Crisanti, P., Blancher, C. & Pessac, B. *A novel cDNA corresponding to transcripts expressed in retina post-mitotic neurons*. *Mechanisms of Development* vol. 43 (1993).

146. Neron, B., Marx, M. & Crisanti, P. *Role of QN1 protein in cell proliferation arrest and differentiation during the neuroretina development*. www.elsevier.com/locate/modo (2001).

147. Nagase, T. *et al. Prediction of the Coding Sequences of Unidentified Human Genes. XIII. The Complete Sequences of 100 New cDNA Clones from Brain Which Code for Large Proteins in vitro the regions causing interruption of protein coding regions*. *DNA RESEARCH* vol. 6 http://www.kazusa.or.jp (1999).

148. Leon, A., Omri, B., Gely, A., Klein, C. & Crisanti, P. QN1/KIAA1009: A new essential protein for chromosome segregation and mitotic spindle assembly. *Oncogene* **25**, 1887–1895 (2006).

149. Wang, W. J. *et al.* CEP162 is an axoneme-recognition protein promoting ciliary transition zone assembly at the cilia base. *Nat Cell Biol* **15**, 591–601 (2013).

150. Nuzhat, N. *et al.* CEP162 deficiency causes human retinal degeneration and reveals a dual role in ciliogenesis and neurogenesis. *Journal of Clinical Investigation* **133**, (2023).

151. Morleo, M. & Franco, B. OFD Type i syndrome: Lessons learned from a rare Ciliopathy. *Biochemical Society Transactions* vol. 48 1929–1939 Preprint at https://doi.org/10.1042/BST20191029 (2020).

152. Pezzella, N., Bove, G., Tammaro, R. & Franco, B. OFD1: One gene, several disorders. *American Journal of Medical Genetics, Part C: Seminars in Medical Genetics* vol. 190 57–71 Preprint at https://doi.org/10.1002/ajmg.c.31962 (2022).

153. Abramowicz, I. *et al.* Oral-facial-digital syndrome type i cells exhibit impaired DNA repair; Unanticipated consequences of defective OFD1 outside of the cilia network. *Hum Mol Genet* **26**, 19–32 (2017).

154. Alfieri, M. *et al.* The centrosomal/basal body protein OFD1 is required for microtubule organization and cell cycle progression. *Tissue Cell* **64**, (2020).

155. Oda, T., Chiba, S., Nagai, T. & Mizuno, K. Binding to Cep164, but not EB1, is essential for centriolar localization of TTBK2 and its function in ciliogenesis. *Genes to Cells* **19**, 927–940 (2014).

156. Lo, C. H. *et al.* Phosphorylation of CEP83 by TTBK2 is necessary for cilia initiation. *Journal of Cell Biology* **218**, 3489–3505 (2019).

157. Cowan, C. S. *et al.* Cell Types of the Human Retina and Its Organoids at Single-Cell Resolution. *Cell* **182**, 1623-1640.e34 (2020).

158. Higginbotham, H., Bielas, S., Tanaka, T. & Gleeson, J. G. *Transgenic mouse line with green-fluorescent protein-labeled Centrin 2 allows visualization of the centrosome in living cells*. *Transgenic Research* vol. 13 (2004).

159. Matsuda, T. & Cepko, C. L. Controlled expression of transgenes introduced by in vivo electroporation. *PNAS* **104**, 1027–1032 (2007).

160. Braun, D. A. & Hildebrandt, F. Ciliopathies. *Cold Spring Harb Perspect Biol* **9**, (2017).

161. Den Hollander, A. I. *et al. REPORT Mutations in the CEP290 (NPHP6) Gene Are a Frequent Cause of Leber Congenital Amaurosis*. *The American Journal of Human Genetics* vol. 79 www.ajhg.org (2006).

162. Landrum, M. J. *et al.* ClinVar: Public archive of interpretations of clinically relevant variants. *Nucleic Acids Res* **44**, D862–D868 (2016).

163. Stenson, P. D. *et al.* The Human Gene Mutation Database (HGMD®): optimizing its use in a clinical diagnostic or research setting. *Human Genetics* vol. 139 1197–1207 Preprint at https://doi.org/10.1007/s00439-020-02199-3 (2020).

164. Abou Tayoun, A. N. *et al.* Recommendations for interpreting the loss of function PVS1 ACMG/AMP variant criterion. *Hum Mutat* **39**, 1517–1524 (2018).

165. Ellard, S. *et al.* ACGS Best Practice Guidelines for Variant Classification 2019. (2019) doi:10.1101/531210.

166. Nykamp, K. *et al.* Sherloc: A comprehensive refinement of the ACMG-AMP variant classification criteria. *Genetics in Medicine* **19**, 1105–1117 (2017).

167. Richards, S. *et al.* Standards and guidelines for the interpretation of sequence variants: A joint consensus recommendation of the American College of Medical Genetics and Genomics and the Association for Molecular Pathology. *Genetics in Medicine* **17**, 405–424 (2015).

168. Preising, M. N. *et al.* Biallelic mutation of human SLC6A6 encoding the taurine transporter TAUT is linked to early retinal degeneration. *The FASEB Journal* **33**, 11507–11527 (2019).

169. Kawalia, A. *et al.* Leveraging the power of high performance computing for next generation sequencing data analysis: Tricks and twists from a high throughput exome workflow. *PLoS One* **10**, (2015).

170. Beck, B. B. *et al.* Mutation of POC1B in a Severe Syndromic Retinal Ciliopathy. *Hum Mutat* **35**, 1153–1162 (2014).

171. Elsayed, S. M. *et al.* Non-manifesting AHI1 truncations indicate localized loss-of-function tolerance in a severe Mendelian disease gene. *Hum Mol Genet* **24**, 2594–2603 (2015).

172. Lek, M. *et al.* Analysis of protein-coding genetic variation in 60,706 humans. *Nature* **536**, 285–291 (2016).

173. Plagnol, V. *et al.* A robust model for read count data in exome sequencing experiments and implications for copy number variant calling. *Bioinformatics* **28**, 2747–2754 (2012).

174. Seelow, D., Schuelke, M., Hildebrandt, F. & Nürnberg, P. HomozygosityMapper - An interactive approach to homozygosity mapping. *Nucleic Acids Res* **37**, (2009).

175. Purcell, S. *et al.* PLINK: A tool set for whole-genome association and population-based linkage analyses. *Am J Hum Genet* **81**, 559–575 (2007).

176. Sante, T. *et al.* ViVar: A Comprehensive Platform for the Analysis and Visualization of Structural Genomic Variation. *PLoS One* **9**, e113800 (2014).

177. Quinodoz, M. *et al.* AutoMap is a high performance homozygosity mapping tool using next-generation sequencing data. *Nat Commun* **12**, (2021).

178. Vangipuram, M., Ting, D., Kim, S., Diaz, R. & Schüle, B. Skin punch biopsy explant culture for derivation of primary human fibroblasts. *J Vis Exp* (2013) doi:10.3791/3779.

179. Pearring, J. N., Spencer, W. J., Lieu, E. C. & Arshavsky, V. Y. Guanylate cyclase 1 relies on rhodopsin for intracellular stability and ciliary trafficking. *Elife* **4**, (2015).

180. Salinas, R. Y. *et al.* Photoreceptor discs form through peripherindependent suppression of ciliary ectosome release. *Journal of Cell Biology* **216**, 1489–1499 (2017).

181. Finkelstein, S. *et al.* Phosphoinositide Profile of the Mouse Retina. *Cells* **9**, (2020).

182. Clark, B. S. *et al.* Single-Cell RNA-Seq Analysis of Retinal Development Identifies NFI Factors as Regulating Mitotic Exit and Late-Born Cell Specification. *Neuron* **102**, 1111-1126.e5 (2019).

183. Das, T., Payer, B., Cayouette, M. & Harris, W. A. *In Vivo Time-Lapse Imaging of Cell Divisions during Neurogenesis in the Developing Zebrafish Retina At the same time, the retina starts its transformation from a morphologically homogeneous neuroepithelium into a tissue consisting of six neuronal and one glial cell types organized into cell type-specific laminae. Asymmetric cell division is thought to be one mecha*. *Neuron* vol. 37 http://www.neuron.org/cgi/ (2003).

184. Cayouette, M. & Raff, M. The orientation of cell division influences cell-fate choice in the developing mammalian retina. *Development* vol. 130 2329–2339 Preprint at https://doi.org/10.1242/dev.00446 (2003).

185. Barton, K. M. & Levine, E. M. Expression patterns and cell cycle profiles of PCNA, MCM6, cyclin D1, cyclin A2, cyclin B1, and phosphorylated histone H3 in the developing mouse retina. *Developmental Dynamics* **237**, 672–682 (2008).

186. Donovan, S. L. & Dyer, M. A. Preparation and square wave electroporation of retinal explant cultures. *Nat Protoc* **1**, 2710–2718 (2007).

187. Kim, K. H. & Sederstrom, J. M. Assaying cell cycle status using flow cytometry. *Curr Protoc Mol Biol* **2015**, 28.6.1-28.6.11 (2015).

188. Darzynkiewicz, Z., Huang, X. & Zhao, H. Analysis of cellular DNA content by flow cytometry. *Curr Protoc Immunol* **2017**, 5.7.1-5.7.20 (2017).

189. Galvin, A. *et al.* Cell Cycle Analysis of Hematopoietic Stem and Progenitor Cells by Multicolor Flow Cytometry. *Curr Protoc Cytom* **87**, (2019).

190. Kosodo, Y. Interkinetic nuclear migration: Beyond a hallmark of neurogenesis. *Cellular and Molecular Life Sciences* vol. 69 2727–2738 Preprint at https://doi.org/10.1007/s00018-012-0952-2 (2012).

191. Baye, L. M. & Link, B. A. Interkinetic nuclear migration and the selection of neurogenic cell divisions during vertebrate retinogenesis. *Journal of Neuroscience* **27**, 10143–10152 (2007).

192. Malicki, J. Cell fate decisions and patterning in the vertebrate retina: The importance of timing, asymmetry, polarity and waves. *Current Opinion in Neurobiology* vol. 14 15–21 Preprint at https://doi.org/10.1016/j.conb.2004.01.015 (2004).

193. Weber, I. P. *et al.* Mitotic Position and Morphology of Committed Precursor Cells in the Zebrafish Retina Adapt to Architectural Changes upon Tissue Maturation. *Cell Rep* **7**, 386–397 (2014).

194. Baye, L. M. & Link, B. A. Nuclear migration during retinal development. *Brain Res* **1192**, 29–36 (2008).

195. Del Bene, F., Wehman, A. M., Link, B. A. & Baier, H. Regulation of Neurogenesis by Interkinetic Nuclear Migration through an Apical-Basal Notch Gradient. *Cell* **134**, 1055–1065 (2008).

196. Baye, L. M. & Link, B. A. Interkinetic nuclear migration and the selection of neurogenic cell divisions during vertebrate retinogenesis. *Journal of Neuroscience* **27**, 10143–10152 (2007).

197. Kumar, D. & Reiter, J. How the centriole builds its cilium: of mothers, daughters, and the acquisition of appendages. *Current Opinion in Structural Biology* vol. 66 41–48 Preprint at https://doi.org/10.1016/j.sbi.2020.09.006 (2021).

198. Reiter, J. & Leroux, M. Genes and molecular pathways underpinning ciliopathies. *Nature Reviews* (2018).